Journal of the European Ceramic Society 41 (2021) 4391–4405

Contents lists available at ScienceDirect

Journal of the European Ceramic Society

journal homepage: www.elsevier.com/locate/jeurceramsoc

Original Article

Understanding the mixed alkali effect on the sinterability and *in vitro* performance of bioactive glasses

Murilo C. Crovace [a,*], Viviane O. Soares [b], Ana Candida M. Rodrigues [a], Oscar Peitl [a], Larissa M. S.C. Raucci [c], Paulo T. de Oliveira [c], Edgar D. Zanotto [a]

[a] Vitreous Materials Laboratory (LaMaV), Department of Materials Engineering, Federal University of São Carlos, São Carlos, SP, Brazil
[b] Department of Sciences, State University of Maringá, Goioerè, PR, Brazil
[c] Cell Culture Laboratory, School of Dentistry of Ribeirão Preto, University of São Paulo, Ribeirão Preto, SP, Brazil

ARTICLE INFO

Keywords:
Bioglass
Sintering
Crystallization
Mixed alkali effect
In vitro bioactivity

ABSTRACT

Bioglass 45S5 is widely known for its ability to regenerate bone. However, this glass cannot be fully densified by viscous flow due to its very high tendency for crystallization. In this work, we evaluate the sintering and bioactivity of Bioglass 45S5-based compositions in which Na_2O is incrementally replaced by K_2O. Our sintering tests demonstrated that the densification of Bioglass 45S5 powders can be significantly enhanced due to a decreased crystallization tendency. The composition in which half of the original Na_2O content was substituted by K_2O exhibits the highest densification rate, evidencing the mixed alkali effect (MAE) in the viscous-flow-driven sintering process. The replacement of Na_2O by K_2O significantly improved both the densification rate and the *in vitro* performance. These results are very relevant for this particular glass and also for the design of new bioactive glasses with improved sinterability.

1. Introduction

Bioactive glasses have been studied for over four decades since Hench [1] developed the gold-standard Bioglass 45S5 and found that it bonds to living tissues. Due to its high osteoconduction and osteoinduction properties [2–4], ability to stimulate angiogenesis [5–7], and antimicrobial activity [8–12], this class of materials presents attractive properties for use in bone regeneration applications.

Understanding the sintering and crystallization behavior of bioactive glasses can sometimes be of critical importance, e.g., in the production of bone scaffolds. However, sintering by viscous flow is often hindered by extensive surface crystallization of the particles, which occurs early in the sintering process [13].

Many attempts have been made to develop new bioactive glasses with improved sinterability; perhaps the most successful case is that of the 13–93 glass [14]. The term "sinterability" refers to the ability of a compact of glass particles to densify by the viscous flow mechanism before crystallization takes place. For any glass, the sintering by viscous flow and the crystallization are concurrent processes; depending on the glass composition one or another will prevail. Frequently, when sintering is improved by compositional changes, the bioactivity is negatively affected and vice-versa. In this view, the development of bioactive glasses with improved sinterability and unchanged or improved bioactivity represents a great challenge.

The search for new strategies to increase the sinterability of Bioglass 45S5 (and also of other bioactive glasses) is of great importance, for example, to obtain mechanically competent scaffolds, especially in the case of replica methods or additive manufacturing techniques such as 3D–printing. Additionally, at low temperatures, sintering can often be driven by viscous flow. Viscous flow-driven sintering has clear advantages over traditional sintering in the solid (crystalline) state.

One potential strategy to increase the stability of Bioglass 45S5 against crystallization seems to be the introduction of potassium in its composition [15,16]. Several bioactive glass compositions containing K_2O are known. Perhaps the best known is the glass S520 ($20.9Na_2O$-$7.1K_2O$-$18CaO$-$52SiO_2$-$2P_2O_5$, mol%), also developed by Hench [17]. This composition shows a lower tendency to crystallize, but it is significantly less bioactive than Bioglass 45S5.

Bellucci et al. [18] tested three CaO-rich compositions, named BG_Ca ($4.6Na_2O$-$45.6CaO$-$47.3SiO_2$-$2.6P_2O_5$, mol %), BG_Ca/K ($4.6K_2O$ -$45.6CaO$-$47.3SiO_2$-$2.6P_2O_5$, mol%) and BG_Ca/Mix ($2.3Na_2O$-2.3-K_2O-$45.6CaO$-$47.3SiO_2$-$2.6P_2O_5$, mol%). In the last two, Na_2O was

* Corresponding author.
E-mail address: mcc@ufscar.br (M.C. Crovace).

https://doi.org/10.1016/j.jeurceramsoc.2020.11.020
Received 14 August 2020; Received in revised form 10 November 2020; Accepted 11 November 2020
Available online 9 January 2021
0955-2219/© 2021 Elsevier Ltd. All rights reserved.

replaced by K_2O to decrease the high crystallization tendency of the glass BG_Ca. Both compositions could be sintered by viscous flow at relatively low temperatures (~ 800 °C). However, *in vitro* tests in SBF showed that small, isolated crystals of hydroxycarbonate apatite (HCA) only started to form after three days, (whereas in the same conditions, the onset for HCA is approximately 6 h in Bioglass 45S5). Even after seven days of immersion in SBF, the glass surface was not completely covered by HCA, indicating considerably lower bioactivity than that of Bioglass 45S5, which has its surface completely covered by an HCA layer in less than 24 h of immersion in SBF [19].

Brink et al. [20] investigated the influence of chemical composition on the *in vivo* bioactivity of 26 different glasses of the Na_2O-K_2O--CaO-MgO-SiO_2-P_2O_5-B_2O_3 system, some of which presented K_2O contents varying between 5 and 15 wt %. They showed that glasses containing K_2O are capable of bonding to bone, similarly to Bioglass 45S5. Brink et al. [21] also developed a glass known as 13–93, which has 7.9 mol % K_2O and some MgO in its composition. This glass has a low tendency to crystallize, making it suitable for sintering and even for fiber drawing. However, its relatively high silica content (54.6 mol %) compared to other bioactive glasses reduces its bioactivity [15].

Salman et al. [22] investigated the effect of substitution of Na_2O by K_2O on the bioactivity of two compositions within the Na_2O-K_2O--CaO-SiO_2-P_2O_5 system. The authors observed a decrease of the bioactivity level and attributed it to partial substitution of Na_2O by K_2O. However, they tested glass-ceramics containing different crystalline phases instead of the precursor glasses.

Although the osteogenic effect of potassium in artificial bone grafts still needs to be better understood, recent studies [23,24] have shown that potassium is associated with an increase in the mineral bone density, and prevents osteoporosis in elderly individuals. Thus, the presence of potassium in bioactive glasses is, in principle, highly desirable.

In this research, we analyzed the effect of the replacement of Na_2O by K_2O on the crystallization kinetics, viscosity and sinterability of Bioglass 45S5. The six best-known glass stability (against crystallization) parameters were calculated to evaluate a possible correlation with the sintering behavior. Moreover, a new sinterability parameter was developed and tested. Finally, the positive effect of replacement of Na_2O by K_2O on the *in vitro* bioactivity is addressed.

2. Experimental

2.1. Glass preparation

Besides the Bioglass 45S5, four additional compositions (Table 1) were formulated via gradual substitution of Na_2O by K_2O. The following reagent grade chemicals were used: sodium carbonate (Na_2CO_3 – JT Baker, USA), potassium carbonate (K_2CO_3 – JT Baker, USA), calcium carbonate ($CaCO_3$ – JT Baker, USA), disodium hydrogen phosphate (Na_2HPO_4 – JT Baker, USA), dipotassium hydrogen phosphate (K_2HPO_4 – JT Baker, USA), and high-purity quartz powder (SiO_2 – Vitrovita, Brazil). The analytical reagents were weighed and homogenized using a jar mill at 150 rpm for 1 h. Two hundred grams of each glass was melted in an electric furnace (Deltech Corp., USA) at 1450 °C for 4 h, using a Pt crucible. The melt was poured on a stainless steel platform and pressed with a stainless steel plaque every 1 h. It was crushed and re-melted over a total of three re-melting procedures to ensure homogeneity. The glass pieces obtained were not annealed to avoid the premature formation of crystalline nuclei since some silicate glasses exhibit high nucleation rates at temperatures close to the glass transition temperature.

Table 1
Nominal compositions (mol %) of the studied glasses.

	Nominal composition (mol%)				
	Na_2O	K_2O	CaO	SiO_2	P_2O_5
100Na/0K (Bioglass 45S5)	24.4	–	26.9	46.1	2.6
75Na/25K	18.3	6.1	26.9	46.1	2.6
50Na/50K	12.2	12.2	26.9	46.1	2.6
25Na/75K	6.1	18.3	26.9	46.1	2.6
0Na/100K	–	24.4	26.9	46.1	2.6

2.2. Density measurements

Bubble-free glass pieces were carefully selected, using a stereo microscope (MZ75 – LEICA, Germany). Density measurements based on Archimedes' principle were carried out with an analytical balance (AB 204 – Mettler Toledo, USA), using ethyl alcohol (PA – Synth, Brazil) as the liquid medium.

2.3. Milling and particle size measurements

All glass compositions were milled in a planetary ball mill (Pulverisette 5 – FRITSCH, Germany), using spherical agate milling media in an agate jar. This procedure is described as follows:

1 Initial crushing of the glass pieces (~200 g) using an agate mortar and pestle;
2 Sieving in a steel sieve with a size of 9 mesh (2 mm);
3 Milling the particles below 2 mm at 550 rpm for 150 s in a planetary ball mill, using 3 agate spheres of 30 mm diameter;
4 Sieving the powder between 25–75 μm (500 and 200 mesh) sieves, with the addition of isopropyl alcohol (99.9 % – JT Baker, USA). Steps 2 and 3 were repeated to obtain a sufficient quantity of powder for the sintering tests (~10 g).

The powder was dried at 120 °C for 2 h. Particle size measurements were carried out in a particle size analyzer (Horiba LA-930, Japan) using anhydrous isopropyl alcohol (99.5 % – JT Baker, USA) as the liquid medium. The refractive indexes of the respective glasses were calculated using the Sciglass database, by the Priven 2000 method.

2.4. Thermal analysis

Differential scanning calorimetry (DSC 404 – Netzsch, Germany) was used to determine the characteristic temperatures (T_g – glass transition temperature; T_x – onset temperature of crystallization; Tc – crystallization peak temperature; T_m – temperature of the melting peak, and T_L – end point of the melting line) of all glass compositions. A Pt pan was used at a heating rate of 50 °C/min, from room temperature up to 1280 °C. This is the highest possible heating rate for this equipment and was employed to simulate the sintering conditions used in sintering experiments, as described below. DSC curves were obtained with 30 mg of glass powders sieved between 25 and 75 μm.

2.5. Sintering

The sintering experiments were carried out *in situ*, using an optical dilatometer (Misura HSM ODHT–Expert System Solutions, Italy) coupled to an image analyzer software. Cylindrical samples with dimensions of approximately 3.2 mm (diameter) by 4.8 mm (height) were used. To ensure good reproducibility, the following procedure was used in the preparation of all samples:

1 75 mg of each powder was weighed out, with particle size in the range of 25–75 μm;
2 The powder was placed into the mold cavity, followed by manual pressing using a system composed of a support and cylindrical steel weights. A total weight of 20 kg was placed over the samples to ensure an applied pressure of 25 MPa. This low pressure was used to minimize fracturing of the particles. No mold lubricant or binder was used.

3 The sample was extracted from the mold and placed on a thin alumina plaque (20 × 10 × 1 mm) with a polished surface. Due to the extreme fragility of the samples, they were carefully slid over the plaque, using a small spatula.
4 The alumina plaque containing the sample was placed over two alumina insulator tubes, which were subsequently slid into the furnace.

The powder was not mixed with binders or any other liquid, because these may induce chemical modification of the particle surfaces or left residues upon heating, thus increasing the number of nucleation sites per unit surface area (Ns).

The heights of the samples were measured while they were still inside the molds, using a caliper rule. The diameter was considered to be the same as that of the pressing rod. The weight of all samples was also determined before sintering. In all sintering measurements, the specimens were pre-heated at 10 °C/min up to 400 °C and kept to equilibrate at this temperature for 10 min. Then, they were heated at 80 °C/min up to 800 °C and cooled down inside the furnace. Images of the samples were captured at every 1 °C increment by a digital camera coupled to the optical dilatometer.

Using the linear and areal shrinkage curves given by the optical dilatometer software, and from the initial relative density of the compact (ρ_0), which was calculated from the initial volume and mass divided by the measured density of the bulk glass, it was possible to calculate the relative density (ρ) of all samples point-to-point during heating, using Eq. 1. This procedure was also used by Durán et al. [25]:

$$\rho = \frac{h_r}{(A_r)^2}\,\rho_0 \tag{1}$$

where h_r is the height of the projected shadow of the sample relative to the initial height h_0 at a given temperature ($h_r = h/h_0$), and A_r is the area of the projected shadow relative to the initial area at a given temperature ($A_r = A/A_0$).

2.6. Scanning electron microscopy (SEM)

After sintering, the samples were embedded in epoxy resin (EpoxiCure® – Buehler, USA) under vacuum, ground with SiC abrasive paper until grit 1200, and then polished using a suspension of CeO_2. Scanning electron microscopy (SEM – Phillips XL-30 TMP, Netherlands) was employed to observe the microstructure of polished transversal sections of the samples coated with gold for 30 s.

2.7. X-ray diffraction (XRD)

The crystalline phases formed in the sintered samples were identified by X-ray diffraction (Rigaku – Ultima IV diffractometer, Japan), using Cu-Kα radiation, within a 2θ range of 10° to 90°, through continuous scans at 0.67°/min. Before the XRD runs, the sintered samples were milled in an agate mortar.

2.8. Viscosity

The viscosity at relatively low temperatures (465–650 °C) was measured using the penetration method [26], with a viscometer developed at the Vitreous Materials Laboratory (LaMaV/UFSCar, Brazil). In this method, a small cylindrical indenter (Ø = 2 mm) made of steel is positioned over a glass disc with diameter Ø = 12 mm and a thickness of 5 mm. Different loads are applied on the indenter, and its penetration velocity into the glass is recorded at a constant temperature. For each temperature, the viscosity (Pa.s) is given by

$$\eta = \frac{0.96\,F}{4\,\pi^{0.5}\,R_i\,V_p} \tag{2}$$

where F is the applied load in Newton, R_i is the indenter radius, and V_p is the penetration velocity in m/s.

2.9. Bioactivity assessment

2.9.1. Bioactivity using acellular SBF solution

For the *in vitro* bioactivity assessment using SBF, the remaining glass was re-melted at 1450 °C/30 min and cast into a cylindrical mold of stainless steel, with a diameter of 12 mm and a height of 35 mm. The glass cylinders were cut into discs with a thickness of approximately 3 mm. The discs were ground with SiC paper until grit 400, using isopropyl alcohol as the liquid medium. Two notches were made on opposite sides of each disc; the notches served as a guide for tying a nylon wire with a diameter of 0.1 mm. The discs were cleaned with isopropyl alcohol in an ultrasonic cleaner for 5 min. After drying, the discs were tied and hanged inside a plastic container containing the SBF-K9 solution, developed by Kokubo [27]. The surface-area-to-volume ratio was kept at 0.1 cm^{-1}. Thus, the plastic containers were placed in a water bath at 36.7 °C for periods of time varying between 1 and 7 days.

After exposure to the SBF solution, the discs were removed and dipped in acetone (99.5 % – Qhemis, Brazil) for 5 s. After drying at room temperature, both flat surfaces were analyzed by Fourier Transform Infrared Spectroscopy (FTIR Spectrum GX – Perkin Elmer, USA).

2.9.2. Bioactivity by assessing the osteogenic potential of pre-osteoblastic cells

For the *in vitro* bioactivity assessment using osteogenic cell cultures, the MC3T3-E1 pre-osteoblastic cells (subclone 14, American Type Culture Collection, Manassas, VA) were cultured in 75 cm^2 flasks with growth medium containing alpha-minimum essential medium (α-MEM, Gibco-Life Technologies, Grand Island, NY), supplemented with 10 % fetal bovine serum (Gibco-Life Technologies), 100 U/ml penicillin (Gibco-Life Technologies), and 100 mg/ml streptomycin (Gibco-Life Technologies). After subconfluence, cells were detached with 1 mM ethylenediaminetetraacetic acid (EDTA) (Gibco-Life Technologies) and 0.25 % trypsin (Gibco-Life Technologies), and then plated at a cell density of 20,000 cells/well on the bioactive glass surfaces placed into 24-well culture plates. The cells were grown with osteogenic medium, composed by growth medium additionally supplemented with 5 mg/ml ascorbic acid (Gibco-Life Technologies) and 7 mM β-glycerophosphate (Sigma–Aldrich, St. Louis, MO), and cultured at 37 °C in a humidified atmosphere of 5 % CO_2 and 95 % air [28].

The culture medium was replaced every 2–3 days, and cells grown on the 100Na/0K group were used as control. At day 21 of culture, cells were washed in Hanks' balanced salt solution (Sigma) and fixed in 70 % ethanol for 60 min at 4 °C. The discs were washed in phosphate-buffered saline and distilled water and stained with 2 % Alizarin Red S (ARS), pH 4.2, for 15 min at room temperature [29].

After being profusely washed in distilled water and let dry overnight, the proportion of ARS-stained area was calculated from the macroscopic images by using the Image Tool software (University of Texas Health Science Center, San Antonio, TX). Discs of the bioactive glasses under the same culture conditions, but without cells, were submitted to the ARS protocol to calibrate the quantitative data. Data were expressed as the proportion of the ARS-labeled area. Statistical analyses were carried out by using the parametric one-way ANOVA test for independent samples, followed by the Holm–Sidak test for multiple comparisons. The level of significance was set at 5 %.

3. Results

3.1. Particle size

The refractive indexes (n_d) of all five compositions of precursor glasses were evaluated using the SciGlass software/database and are shown in Table 2. The particle size distribution curves for all powders,

Table 2
Mean particle size (D_{med}) for the precursor glasses 100Na/0K to 0Na/100K milled at 550 rpm/150 s. The calculated (see text) refractive indexes (n_d) are also shown.

Glass composition	Calculated n_d (at 20 °C)	D_{med} (μm) ± 2 μm
100Na/0K (Bioglass 45S5)	1.571	52
75Na/0K	1.574	46
50Na/50K	1.576	48
25Na/75K	1.578	44
0Na/100K	1.580	47

obtained using the procedure described in item 2.3, are shown in Fig. 1. The frequency distribution curves are similar, showing only small differences for the compositions 100Na/0K and 0Na/100K. Although the powders were sieved between 25 and 75 μm, some particles were out of this range. The powder with the composition 0Na/100K exhibits the highest quantity of fine particles (below 20 μm). The values for the mean particle size were 52 μm for the composition 100Na/0K and 44 μm for the composition 25Na/75K, with a total variation of approximately 8 μm. For a better comparison, all values of the mean particle sizes are shown in Table 2.

3.2. Thermal analysis

As observed in the DSC curves (Fig. 2), the substitution of Na_2O by K_2O decreases the intensity and broadens the crystallization peak from 100Na/0K (Bioglass– 45S5) up to the composition 25Na/75K. The intensity of the crystallization peak increases again for the composition without Na_2O (0Na/100K), but it remains lower than the intensity observed for the composition 100Na/0K. The same tendency is observed for the melting peak (T_m): a decrease of T_m (both T_{m1} and T_{m2}) is observed up to the composition 25Na/75K, increasing again for the composition 0Na/100K. There is no clear tendency for the onset temperature of crystallization (T_x); the values of T_x oscillate between 654 °C (composition 25Na/75K) and 714 °C (composition 0Na/100K). For a better analysis, the values of the characteristic temperatures of these glasses are shown in Table 3.

Concerning T_g, the substitution of Na_2O by K_2O causes an interesting effect (Fig. 3). Initially, T_g decreases from 540 °C to 519 °C (composition 75Na/25K), reaching a minimum value (515 °C) for the composition 50Na/50K. Then, it increases for the compositions 25Na/75K and 0Na/100K (521 °C and 542 °C, respectively).

This behavior of T_g is a signature of a phenomenon known as *mixed alkali effect* (MAE), which has also been observed in several other systems [30–32]. It has been experimentally proven that when an alkali is

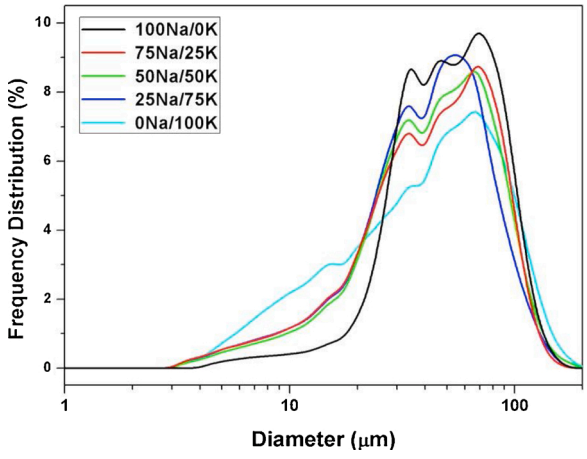

Fig. 1. Frequency distribution curves of particle diameter for all 5 investigated glasses, with different Na/K ratio, milled in a planetary ball mill at 550 rpm for 150 s.

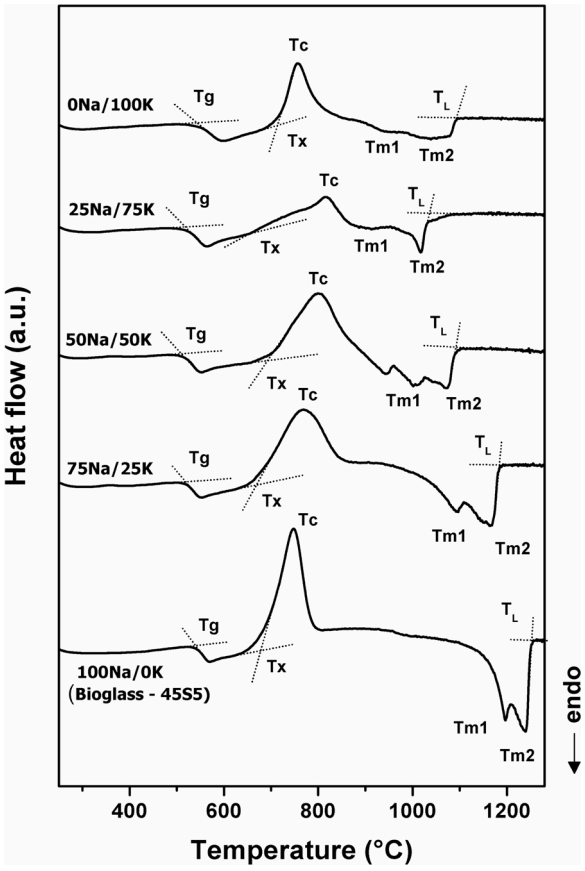

Fig. 2. DSC curves of the glass compositions 100Na/0K (Bioglass 45S5), 75Na/25K, 50Na/50K, 25Na/75K, and 0Na/100K, at a heating rate of 50 °C/min.

Table 3
Characteristic temperatures of the glass compositions 100Na/0K (Bioglass 45S5), 75Na/25K, 50Na/50K, 25Na/75K, and 0Na/100K, determined from the DSC curves. These values have an imprecision of approximately 5 °C.

Composition	T_g (°C)	T_x(°C)	T_c(°C)	T_{m1} (°C)	T_{m2} (°C)	T_L (°C)
100Na/0K (Bioglass 45S5)	540	678	748	1197	1240	1250
75Na/25K	519	669	769	1096	1164	1181
50Na/50K	515	696	799	1002	1071	1089
25Na/75K	521	654	817	913	1018	1037
0Na/100K	542	714	756	983	1039	1093

substituted by another, some properties undergo nonlinear variations, with maxima and minima for compositions with a ratio 1/1 of each alkali ion. These minima/maxima become more pronounced as the difference alkali ions radius becomes greater. This effect is especially notable in cases of transport phenomena, which are dependent on the ionic mobility, such as viscous flow, crystallization, and electrical conductivity, among others. The MAE on T_g and other physical properties, such as dilatometric softening point and Vickers hardness, has already been reported by Tylkowski [15] for Bioglass-based compositions in which Na_2O was replaced by K_2O.

One or more of the well-known glass stability (GS) parameters are commonly used to compare the stability of different glass compositions against crystallization. These glass stability parameters provide a tool that can give valuable information about the resistance of a particular glass to crystallize on heating. GS parameters are traditionally used to compare the crystallization behavior of stoichiometric glasses and could assist in the development of off-stoichiometric, multicomponent glasses that exhibit higher sinterability, compositions for fiber drawing, and

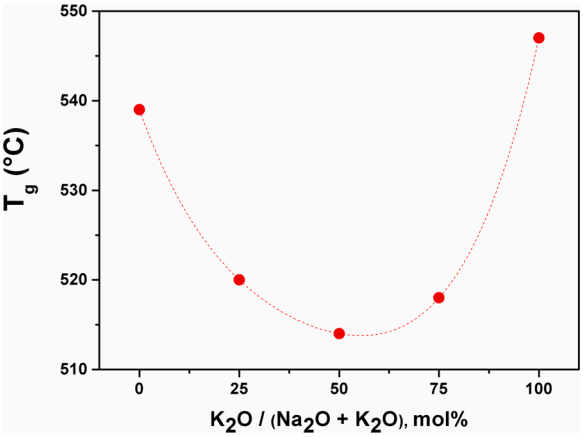

Fig. 3. Glass transition temperature (T_g) as a function of the percentage of K_2O/Na_2O substitution in Bioglass 45S5.

bulk metallic glasses, among other applications [33].

Several parameters have been proposed to describe glass stability. The most common of these are shown in Table 4. The GS parameters are calculated in a straightforward manner from the characteristic temperatures (Table 5) obtained in DSC or DTA measurements.

The parameter K_2 is often used to provide an idea of the "sintering window" or "processing window" [39–41], i.e., a temperature range where the viscosity allows for fast viscous flow sintering without undesired crystallization. K_2 has been employed to evaluate the sinterability of certain bioactive glasses. For comparison, the calculated values of the six GS parameters, K_T, K_2, K_w, K_{LL}, K_H, and K_{SP}, for all compositions are shown in Table 5. These parameters are calculated using the characteristic temperatures in Kelvin. The values shown in this table are dimensionless, except K_2 and K_{SP}, which are given in Kelvin. The higher the values of these parameters, the higher is the glass stability against crystallization on the heating path.

According to the parameter K_T, GS increases as Na_2O is replaced by K_2O, reaching a maximum value for the composition 25Na/75K. The parameter K_2 indicates that the composition 50Na/50K shows a lower tendency to crystallize ($K_2 = 181 \pm 4$K), followed by the composition 0Na/100K ($K_2 = 172 \pm 4$K). According to this parameter, the composition 25Na/75K has the lowest GS, i.e., the highest tendency for crystallization. Like K_2, K_w, and K_{LL}, the parameter K_H also indicates that the compositions 50Na/50K and 0Na/100K exhibit the highest glass stability, since the values of K_H are similar (0.46 and 0.45 ± 0.03, respectively). To facilitate the visualization of MAE phenomena, the values for each GS parameter were plotted against composition (Fig. 4). As seen in Fig. 4, only the parameters K_T and K_{SP} show a curve typical of the MAE, exhibiting a clear maximum value for an intermediate composition; however, both fail in the prediction of the most sinterable composition, as discussed further. In addition to K_2 and K_H, the parameters K_w and K_{LL} also indicate that the compositions 50Na/50K and 0Na/100K exhibit the highest GS values, as is seen in Fig. 4 – *c* and *d*.

Unlike the parameter K_2, K_{SP} indicates that the composition 25Na/75K exhibits the highest glass stability; the value of K_{SP} for the composition 25Na/75K is close to the value obtained for the composition 50Na/50K: 27.3 ± 0.1K and 23.7 ± 0.1K, respectively. The value of K_{SP} obtained for the composition 0Na/100K (8.9 ± 0.1K) is inferior to the values found for Bioglass 45S5 ($K_{SP} = 11.9 \pm 0.1$K) and for the composition 75Na/25K ($K_{SP} = 18.9 \pm 0.1$K).

Table 4
Most common glass stability parameters and their respective authors [34].

Parameter	Author(s)
$K_T = T_g / T_L$	Turnbull [35]
$K_2 = T_x - T_g$	Angell [34]
$K_w = (T_x - T_g) / T_m$	Weinberg [36]
$K_{LL} = T_x / (T_g + T_L)$	Lu and Liu [33]
$K_H = (T_x - T_g) / (T_m - T_x)$	Hrüby [37]
$K_{SP} = (T_x - T_g) (T_c - T_x) / T_g$	Saad and Poulain [38]

3.3. Sintering

To verify that the substitution of Na_2O by K_2O, in fact, improves the sinterability of Bioglass 45S5, pellets of the five glasses were analyzed in an optical dilatometer, as described previously.

As explained in item 2.5, after measurements in the optical dilatometer, Eq. 1 was used to obtain the relative density as a function of temperature. Thus, it was necessary to know the density of all glasses. Table 6 shows the experimental values of density, and those calculated using SciGlass (method Priven 2000). The experimental and calculated values of density are in good agreement. The only exception is for composition 0Na/100K, whose experimental density is smaller than the calculated value. Using Doweidar's model, Tylkowski et al. [15] also observed a deviation of the calculated densities for glasses containing high levels of potassium. The substitution of Na_2O by K_2O decreased the glass density since potassium, despite its higher atomic weight, is a network modifier ion with a larger ionic radius than sodium. Therefore, it increases the glass molar volume [15], resulting in a more open network structure.

Fig. 5 shows the estimated relative density (Eq. 1) as a function of temperature, for powders sieved between 25 and 75 μm. Each curve corresponds to the arithmetic mean of three different samples (point-to-point), and the error bars represent the resulting standard deviations. The measurements were interrupted after saturation for each composition.

The temperatures at which densification starts (T_{onset}), the maximum relative densities or densities of saturation (ρ_{sat}), and the temperatures corresponding to the saturation density (T_{sat}) for all compositions are shown in Table 7.

The shrinkage process for Bioglass 45S5 starts at 550 °C (T_{onset}), reaching saturation at approximately 630 °C (T_{sat}). The powder compact densifies only 4 %, from 0.57 (ρ_0) to 0.61 (ρ_{sat}). For the composition 75Na/25K, densification starts at 530 °C and saturation is also reached at 630 °C; however, the relative density reaches 0.69, i.e., 11 % densification.

The composition 50Na/50K reached the highest value of relative density, 0.81. This corresponds to a densification of approximately 23 %. In this case, saturation occurs at 650 °C.

With the subsequent exchange of Na_2O by K_2O, the maximum relative density undergoes a drastic reduction for the compositions 25Na/75K and 0Na/100K, reaching 0.64 and 0.60, respectively. The composition 0Na/100K shows the highest onset temperature (~ 600 °C); furthermore, this glass densified less than 3 %, a value inferior to that observed for Bioglass 45S5. The subtle reduction of relative density, observed from 500 °C up to 600 °C for the composition 0Na/100K, is related to the high thermal expansion coefficient (TEC) of this glass. This means that the powder compact undergoes a detectable expansion in this temperature range. An increase in TEC with the addition of K_2O is an expected result; several papers have reported such an increase in silicate glasses and glass-ceramics due to the addition of this oxide [42–44].

3.4. SEM

After sintering in an optical dilatometer at 80 °C/min up to the corresponding saturation temperature, SEM images were taken from all investigated samples. The images *a* and *b* in Fig. 6 attest to the low stability of Bioglass 45S5 against crystallization. All particles are fully crystallized and still show an irregular shape, with sharp edges, indicating that viscous flow was readily interrupted. It is known that this glass exhibits internal nucleation for certain heat treatments. However, for the current non-isothermal runs, the crystallization fronts from the

Table 5
Values of stability parameters for the compositions 100Na/0K (Bioglass 45S5), 75Na/25K, 50Na/50K, 25Na/75K, and 0Na/100K. K_2 and K_{SP}, in Kelvin. An imprecision of 5 °C in each temperature was considered for error calculations.

Composition	K_T	K_2 (K)	K_W	K_{LL}	K_H	K_{SP} (K)
100Na/0K (Bioglass - 45S5)	0.534 ± 0.004	138 ± 4	0.09 ± 0.03	0.407 ± 0.004	0.24 ± 0.04	11.9 ± 0.1
75Na/25K	0.545 ± 0.004	150 ± 4	0.10 ± 0.03	0.419 ± 0.004	0.29 ± 0.03	18.9 ± 0.1
50Na/50K	0.579 ± 0.004	181 ± 4	0.13 ± 0.02	0.451 ± 0.004	0.46 ± 0.03	23.7 ± 0.1
25Na/75K	0.606 ± 0.004	133 ± 4	0.10 ± 0.03	0.441 ± 0.004	0.35 ± 0.04	27.3 ± 0.1
0Na/100K	0.597 ± 0.004	172 ± 4	0.13 ± 0.02	0.453 ± 0.004	0.45 ± 0.03	8.9 ± 0.1

Note: The underlined numbers refer to the maxima of each parameter.

surface meet before any crystal is formed in the interior of the particles.

For the composition 75Na/25K, the particles are more rounded (Fig. 6 *c – d*), indicating that viscous flow occurred. The proximity of particle centers confirms that they underwent some densification, but sintering was also interrupted by the formation of a crystallized layer at the particles surfaces (Fig. 6 – *d*). However, the crystalline layer formed here is thinner than that formed on Bioglass 45S5.

As mentioned previously, the composition 50Na/50K showed the highest value of saturation density (0.81). As seen in Fig. 6 *e – f*, the particles exhibit a round shape and a superior number of contact points, indicating that viscous flow occurred to a great extent. The formation of a thin, crystallized layer at the particle surface (Fig. 6 – *f*) also halts the densification process. In addition to the crystallized layer, crystals were also identified inside the sintered particles.

The compositions 25Na/75K (Fig. 6 *g – h*) and 0Na/100K (Fig. 6 *i – j*) show similar SEM micrographs: there are few contact points between particles, which exhibit irregular shapes with sharp edges. Rapid surface crystallization hindered the viscous flow process. For the composition 25Na/75K (Fig. 6 – *h*), in addition to the crystallized layer, a large number of crystals can be observed inside the particles. These crystals, which were formed during a short period, indicate that this composition exhibits a high nucleation rate. The particles of composition 0Na/100K also have crystals in the volume. However, these have an acicular shape (Fig. 6 – *j*).

3.5. XRD

To identify the crystalline phases formed at the particle surfaces, two sintered samples of each composition were prepared as described in item 2.7 and analyzed by XRD. The XRD patterns obtained are shown in Fig. 7. The XRD pattern of sintered Bioglass 45S5 (100Na/0K) confirms that a highly-crystallized fraction was formed in this glass during the sintering test, with the formation of $Na_2CaSi_2O_6$ (ICDD 77–2189 PDF#2). The other compositions show a halo, characteristic of an amorphous phase. In the 75Na/25K composition also, the main crystalline phase is $Na_2CaSi_2O_6$. In the compositions 25Na/75K and 0Na/100K, calcium potassium silicate (K_2CaSiO_4 – ICDD 19–943 PDF#2) is the major phase, which is responsible for the saturation of densification in both these glasses. Two different crystalline phases ($Na_2CaSi_2O_6$ and K_2CaSiO_4) coexist in the composition 50Na/50K.

3.6. Viscosity

To understand the sintering process more comprehensively, i.e., not only from the glass crystallization perspective, we also determined the viscosity of all glasses by a penetration method (see item 2.8). For each composition, the viscosity was calculated point-to-point using Eq. 2, and then plotted against temperature. Measurements were made for viscosities in the range of 10^{12} to 10^{13} Pa.s (in the vicinity of T_g) down to 10^7 Pa.s, which for these glasses corresponds to approximately 100 °C above T_g. In this viscosity range, sintering by viscous flow occurs in the studied compositions. At higher temperatures, i.e., lower viscosities, the penetration velocity is too high to be followed. As shown in Fig. 8, the MAE is again evident, as previously inferred from the T_g values for these glasses. The viscosity of Bioglass 45S5 drops as sodium is substituted by potassium, whereas the viscosities of the compositions 75Na/25K and 25Na/75K are very close. As expected from the T_g experiments, the composition 50Na/50K exhibits the lowest viscosity. The viscosity of the composition without sodium (0Na/100K) is much higher than that of Bioglass 45S5 (Fig. 8).

3.7. Bioactivity assessment

Bioactivity tests were performed in SBF to analyze the influence of the substitution of Na_2O by K_2O on the onset time for crystallization of a hydroxycarbonate apatite (HCA) layer on the glass surfaces. After different exposure times to the SBF solution, the surface changes were followed by FTIR. The peaks of interest are located at 560 and 602 cm^{-1}. These are attributed to the P—O bond and are related to the crystallization of HCA.

The spectra in Fig. 9 show the evolution of the superficial transformations occurring in the compositions 100Na/0K (Bioglass 45S5), 75Na/25K, 50Na/50K, 25Na/75K, and 0Na/100K, as a function of time.

The natural vibrational mode of the non-reacted surfaces (0 h of exposure to SBF) is altered as a function of the time of exposure to the SBF solution. After 1 h, the formation of a silica gel layer (corresponding to stage III of the mechanism of HCA formation, described by Hench [4]) can be noted for all compositions. The existence of the silica-rich layer is confirmed by the presence of two peaks at 1250 and 1095 cm^{-1}, related to the stretching of the Si-O-Si bond. Additional confirmation is provided by the sharpening of the peak at 470 cm^{-1}, also related to the Si-O-Si bond. The peak at 930 cm^{-1}, attributed to the Si-O bond and present in the spectra of non-reacted materials, disappears during the process of repolymerization. It can also be observed that an amorphous calcium phosphate ($CaO\text{-}P_2O_5$) layer was formed after only 1 h of exposure. The formation of amorphous Ca-P corresponds to stage IV, and it is characterized by a broad peak at 560 cm^{-1}.

As the reaction time increases, the broad peak at 560 cm^{-1} sharpens and is later divided into two peaks at 602 and 560 cm^{-1}, related to the P—O bond. The splitting into two peaks indicates the beginning of crystallization of the amorphous Ca-P, leading to the formation of HCA. Simultaneously, the formation of a crystalline HCA layer leads to the formation of a peak related to the stretching of the P—O bond at 1050 cm^{-1} (samples with 12 h of exposure to SBF).

The peak corresponding to the Si-O-Si bond at 470 cm^{-1} persists until 12 h of exposure to SBF, indicating the presence of a small amount of silica gel that has not yet been fully covered by the amorphous Ca-P layer. The only exception is the composition 0Na/100K, whose peak at 470 cm^{-1} can still be identified after 24 h of exposure. After 24 h of exposure to SBF, the peaks related to HCA dominate the spectra for all glasses tested.

The results of the matrix mineralization assay revealed that at day 21 of culture, MC3T3-E1 cells laid down an ARS-stained matrix over the entire disc surface in all glass compositions tested. The macroscopic imaging of cultures depicted dark-brownish areas of irregular contour and varied dimensions on a more homogeneous reddish violet background. The quantitative analysis revealed that the cultures grown on the 75Na/25K glass exhibited the highest percentage of matrix

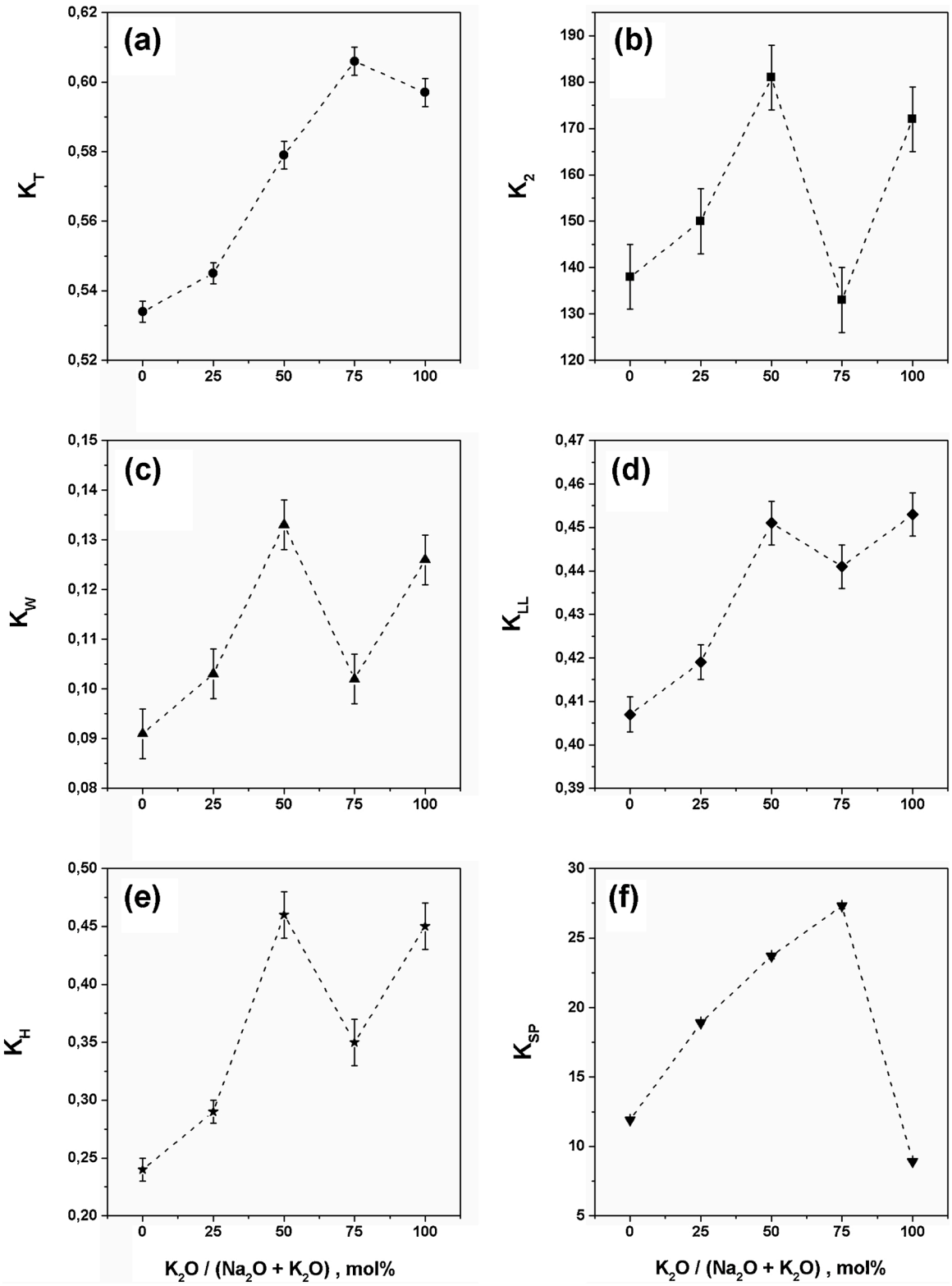

Fig. 4. Glass stability parameters (K_T (*a*), K_2 (*b*), K_W (*c*), K_{LL} (*d*), K_H (*e*), and K_{SP} (*f*)) as a function of composition.

mineralization, followed by the ones on 50Na/50K. Both compositions supported a higher osteogenic potential of MC3T3-E1 cells than the 100Na/0K and 0Na/100K glasses (Fig. 10, one-way ANOVA, Holm–Sidak test, $P < 0.05$).

4. Discussion

Previous studies [45–47] have shown that viscous flow sintering of Bioglass 45S5 powder is hindered by extensive crystallization during heating, leading to a powder compact composed of loosely bonded and partially crystalline particles. This is the reason why in the fabrication of bone scaffolds [48–51], for example, Bioglass 45S5 is usually sintered at

Table 6
Density for the compositions 100Na/0K (Bioglass 45S5), 75Na/25K, 50Na/50K, 25Na/75K, and 0Na/100K, measured and calculated using SciGlass (Priven's 2000 method).

Composition	Experimental density (g/cm^3)	Calculated density (g/cm^3) – from SciGlass	Calculated surface energy (γ) at 550 °C (J/m^2) – from SciGlass
100Na/0K (Bioglass 45S5)	2.70 ± 0.01	2.72	0.343
75Na/25K	2.69 ± 0.01	2.70	0.313
50Na/50K	2.68 ± 0.01	2.69	0.284
25Na/75K	2.66 ± 0.01	2.69	0.262
0Na/100K	2.64 ± 0.01	2.69	0.243

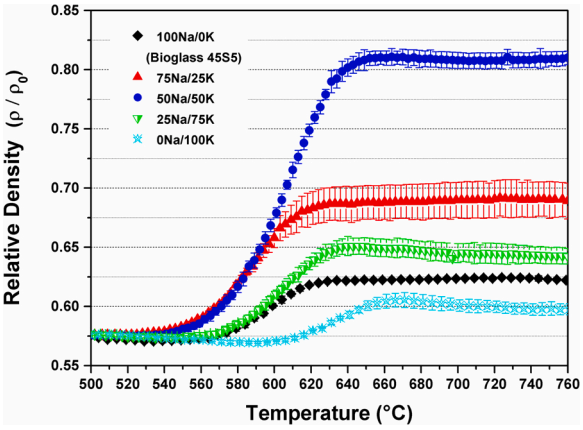

Fig. 5. Relative density (estimated after Eq. 1) as a function of temperature, for the glasses 100Na/0K, 75Na/25K, 50Na/50K, 25Na/75K, and 0Na/100K. The sintering experiments were performed in an optical dilatometer, with a heating rate of 80 °C/min. The particle size distribution was in the range 25–75 μm.

Table 7
Onset temperature of sintering (T_{onset}), saturation temperature of sintering (T_{sat}), and density at saturation (ρ_{sat}) for the compositions 100Na/0K (Bioglass 45S5), 75Na/25K, 50Na/50K, 25Na/75K, and 0Na/100K.

Composition	T_{onset} (°C)	T_{sat} (°C)	ρ_{sat}	Sintering rate - d(ρ/ρ0)/dT (°C^{-1})
100Na/0K (Bioglass 45S5)	550	630	0.61	10.3×10^{-4}
75Na/25K	530	630	0.69	19×10^{-4}
50Na/50K	530	650	0.81	32×10^{-4}
25Na/75K	560	640	0.64	13×10^{-4}
0Na/100K	600	660	0.60	6×10^{-4}

high temperatures (T ≥ 900 °C), at which the glass particles are already fully crystallized [48,52]. Hence, the sintering process occurs by atomic transport in the solid (crystalline) state, not by viscous flow.

The relatively low content of glass network formers (silica and P_2O_5) in Bioglass 45S5 (compared to normal commercial silicate glasses) explains its crystallization tendency. In practical processing conditions, crystalization hinders the sintering process by viscous flow. This is a problem for most bioactive glasses whose compositions have a low content of network formers, i.e., reduced network connectivity. On the other hand, a higher content of network modifiers is important because they increase the glass solubility and bioactivity, which is vital for such types of glasses.

In many studies, the enhanced sinterability of many glass compositions has been related to an increase of the network connectivity [16,53]. However, given that the content of network formers is kept constant among all compositions analyzed in this work ($SiO_2 + P_2O_5 = 48.7$ mol %), the MAE on sintering cannot be explained in terms of network connectivity.

Viscous-flow-driven densification with concurrent crystallization is a complex phenomenon. It depends on several parameters which are either composition-dependent, such as the crystal growth rates (U), viscosity (η), and glass-vapor surface energy (γ), or processing-controlled, such as the initial density of the powder compact (ρ_0), average particle size (r), number of preferential sites for surface nucleation (N_S), temperature (T) and time (t) of heat-treatment, as well as the heating rate (since processing is usually non-isothermal). Experimental observations reinforced by model calculations [54–56] have shown that high temperatures, high values of liquid-air surface energy, and low values of viscosity, crystal growth rate, N_s, and particle size will favor the viscous flow sintering process over crystallization for any glass composition.

4.1. Effects on the sinterability and glass stability

The powder preparation procedure described in item 2.3 ensures a similar particle size distribution for all glasses (as seen in Fig. 1), which in turn leads to similar initial packing densities (ρ_0). N_s depends on the number of defects present at the surface of the particles generated during the milling process, which serve as preferential sites for the nucleation of crystals. Müller et al. [57] showed that N_s does not vary significantly with temperature or time of heat-treatment; therefore, N_s is considered to be "athermic", being practically constant during the sintering process. Typical values for milled glass powders lie in the range 10^9 – 10^{11} nucleation sites/m^2 [57]. Therefore, as long as the milling procedure was the same, a constant N_s for all compositions is a consistent assumption.

Other processing-controlled parameters, such as heating and cooling rates, were also kept constant. Therefore, only composition-dependent parameters are believed to significantly affect the sintering kinetics in this research work.

Since Bioglass 45S5 is known for its low stability against crystallization, the maximum heating rate allowed by our equipment (80 °C/min) was employed to minimize crystallization. Despite the high heating rate employed, the powder compact densified only 4 % (relative density changed from 0.57 to 0.61). While the experimental density of Bioglass 45S5 is approximately 2.70 g/cm^3 (Table 6), the density of the $Na_2CaSi_2O_6$ crystal is approximately 2.81 g/cm^3, which gives a difference of 4 %. Therefore, the observed shrinkage is mainly due to crystallization. This is proven by the SEM images (Fig. 6 – *a* and *b*), in which all the particles are crystalline and present sharp edges. This indicates that surface crystallization occurred before the viscous flow. Additionally, the pellets were highly friable after heat-treatment for sintering.

After the sintering experiments, the glasses 75Na/25K and 50Na/50K exhibited somewhat rounded particles and the formation of neck between particles (Fig. 6 – *c* to *f*). This is especially true for the 50Na/50K glass, which showed the highest sinterability. These observations allow us to conclude that both compositions underwent viscous flow before significant crystallization.

Fig. 6 (*g* – *h*) shows that despite the high heating rate used, a large number of crystals are formed inside particles of the 25Na/75K glass. Isolated crystals were also observed in the interior of particles of the 0Na/100K glass (Fig. 6 *i* – *j*).

Similar to Bioglass 45S5, the particles of both 25Na/75K and 0Na/100K compositions still exhibit sharp edges and few contact points. Although these compositions have a lower tendency to crystallize, since the particles are not fully crystallized, the high viscosity did not allow for viscous flow. Furthermore, Fig. 6 – *j* shows a thin, crystallized layer formed on the surface of 0Na/100K particles, which also hinders the sintering by viscous flow.

The SEM micrographs in Fig. 6 (a–b) reveal a thick, crystalline layer of $Na_2CaSi_2O_6$ formed on the surfaces of particles of the composition

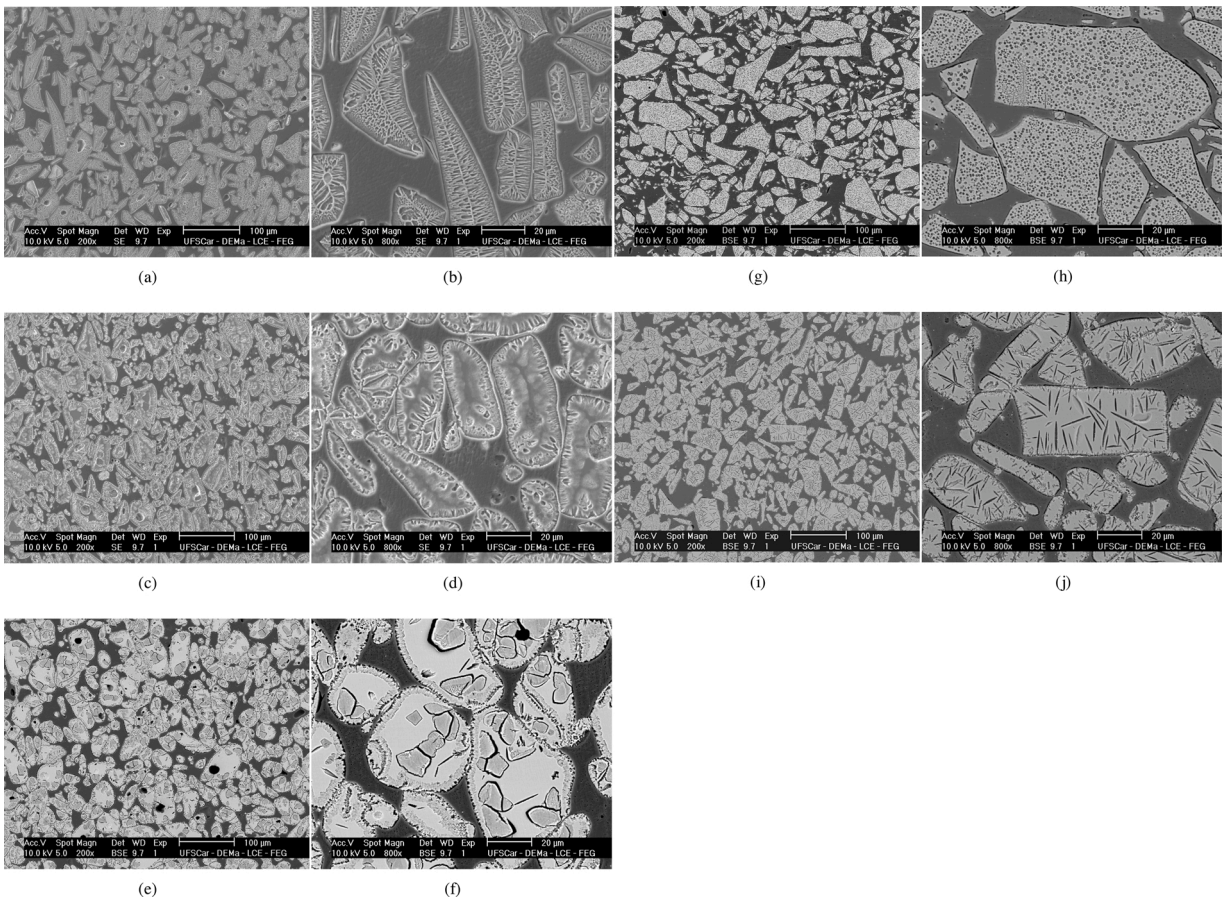

Fig. 6. SEM micrographs of the glasses 100Na/0K (*a-b*), 75Na/25K (*c-d*), 50Na/50K (*e-f*), 25Na/75K (*g-h*), and 0Na/100K (*i-j*) sintered in an optical dilatometer at 80 °C/min up to the corresponding saturation temperature. The particle sizes were in the range 25−75 μm.

100Na/0K (Bioglass 45S5). The SEM micrographs of Fig. 6 also reveal that as Na_2O is replaced by K_2O, the thickness of the surface crystalline layer decreases. If N_s is considered to be approximately the same for all compositions (since the milling procedure was the same), it can be concluded that the K_2CaSiO_4 phase, found in the K_2O-rich compositions, probably has a lower crystal growth rate than the $Na_2CaSi_2O_6$ phase.

The density at saturation as a function of the quantity of Na_2O replaced by K_2O follows a typical MAE behavior, with a maximum value for the composition 50Na/50K (Fig. 11). The slope of the linear part of the curves of relative density versus composition represents the rate of densification or sintering. The rate of sintering for each composition is shown in Table 7; a maximum is obtained for the composition 50Na/50K (32×10^{-4} °C^{-1}). If the sintering rate is plotted against the composition, once more a MAE behavior is observed (Fig. 11). Thus, it is clear that the 50Na/50K glass not only reached a higher density at saturation, but also sintered faster.

To evaluate the sinterability of glass powders, Prado et al. [58] proposed and successfully tested a general parameter, S, given by:

$$S(T) = \frac{\gamma}{\sqrt{N_s}\, U(T)\, \eta(T)\, r} \tag{3}$$

where γ is the supercooled liquid-air surface energy, N_S is the density of nucleation sites on the glass particles surface, U(T) is the crystal growth rate, η(T) is the viscosity, and r is the average particle size. For shallow supercoolings, i.e., relatively high temperatures ($T \geq 0.85T_m$), an approximate expression (S_{hT}) was developed:

$$S_{hT}(T) = \frac{2\pi\, \gamma\, N_A\, (T_m)^2\, \sqrt[3]{V_m^2}}{10\sqrt{N_s}\, r\, \Delta H_m\, \Delta T^2} \tag{4}$$

where N_A is Avogadro's number, T_m is the melting temperature of the crystal phase, V_m is the molar volume, ΔH_m is the enthalpy of fusion of the crystal phase, and $\Delta T = T_m - T$ is the undercooling. This parameter avoids the need to determine U(T) and η(T), which are difficult and require time-consuming experiments. Additionally, it allows one to predict whether a given glass will substantially densify or if crystallization will hinder viscous flow and densification.

However, in the case of the Bioglass-based compositions, sintering takes place at low temperatures, just above T_g. Additionally, the enthalpies of melting of $Na_2CaSi_2O_6$ and K_2CaSiO_4 phases are unknown. Therefore, a new equation valid for deep undercoolings is required.

If we consider that the Stokes-Einstein-Eyring (SEE) equation $D_\eta = \frac{k_B T}{\lambda \eta}$ is valid, and therefore $D_U \cong D_\eta$, in most practical cases the crystal growth rate, U(T), can be expressed by the Screw Dislocation mechanism (please check reference [58] for more details):

$$U(T) = f \frac{k_B T}{\lambda\, \eta_G}\left[1 - \exp\left(-\frac{\Delta G}{RT}\right)\right] \tag{5}$$

where f is the fraction of preferred growth sites on the crystal-liquid interface (that is smaller than unity), k_B is the Boltzmann constant, λ is the (unknown) diameter of the diffusing structural units, η_G is considered here as the viscosity of the residual glassy phase, ΔG is the difference in the Gibbs free energy between the crystal and the undercooled liquid, R is the gas constant and T the temperature.

At deep undercoolings, where viscous flow sintering of the present glasses occurs ($T \sim 0.54$–$0.70\ T_m$), the exponential term in the Eq. 5 tends to zero. Moreover, if one considers that λ is the same for all these compositions, the difference regarding U(T) among distinct glass

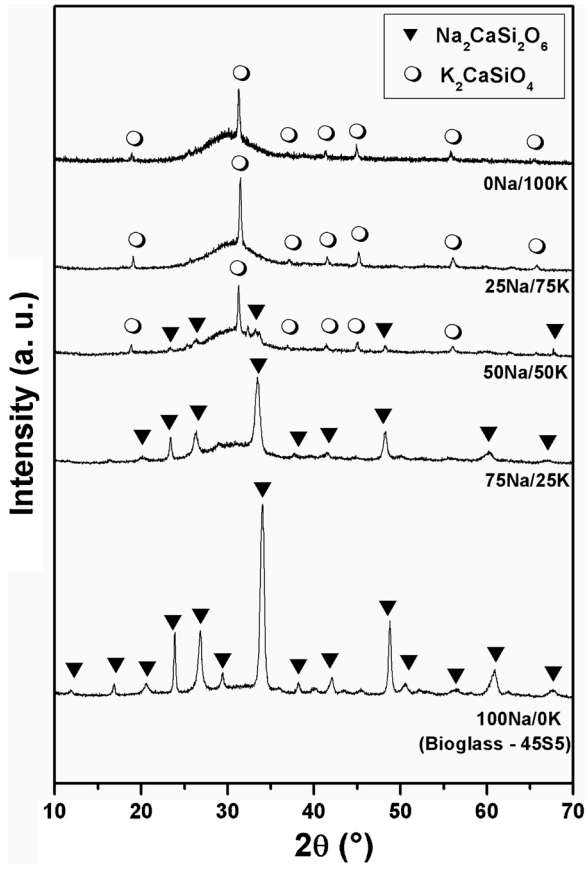

Fig. 7. XRD spectra of the compositions 100Na/0K (Bioglass 45S5), 75Na/25K, 50Na/50K, 25Na/75K, and 0Na/100K sintered in an optical dilatometer at 80 °C/min up to the density saturation temperature.

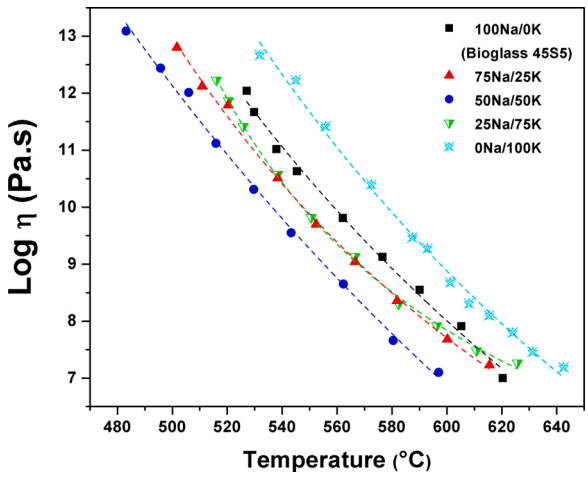

Fig. 8. Experimental viscosity values against temperature, obtained by the penetration method, for the compositions 100Na/0K (Bioglass 45S5), 75Na/25K, 50Na/50K, 25Na/75K, and 0Na/100K.

compositions can be approximated by:

$$\Delta U(T) = \frac{f\ T}{\eta_G} \tag{6}$$

The parameter *f*, in turn, can be approximated by $(T_L\text{-}T)/T_L$, where T_L is the liquidus temperature (for non-stoichiometric compositions). Then, Eq. 6 can be rewritten as:

$$\Delta U(T) = \frac{(T_L - T)\ T}{T_L\ \eta_G} \tag{7}$$

Substituting Eq. 7 in the Eq. 3, and considering N_S constant (since the milling and sieving procedure employed was the same for all glasses), a modified sinterability parameter (S_{LT}), can be derived for deep supercoolings, i.e., low temperatures:

$$S_{LT}(T) = \frac{\gamma\ T_L}{(T_L - T)\ T\ r} \tag{8}$$

As mentioned before, Eq. 5 describes quite well U(T) at low undercoolings but is not valid for temperatures close to T_g ($T \leq 1.3T_g$). Indeed, a plethora of studies shown that below a certain decoupling temperature (T_d), the mechanism of diffusion controlling crystal growth can no longer be described by the viscosity ($D_U \neq D_\eta$); i.e., the SEE equation fails in predicting the crystal growth kinetics. Thus, to compare all compositions regarding S_{LT}, we considered a sintering temperature $T \approx T_d$. In this case, the sinterability parameter (Eq. 8) becomes:

$$S_{LT}(T) = \frac{\gamma\ T_L}{(T_L - T_d)\ T_d\ r} \tag{9}$$

For many silicate glass compositions, T_d lies in the range 1.03-1.30T_g [59]. Therefore, to use Eq. 9, we can take the most typical values of $T_d = 1.15T_g$ and $T_d = 1.25T_g$ as lower and upper bounds for S_{LT}, respectively. Then, the calculated values of S_{LT} for glasses 100Na/0K, 75Na/25K, 25Na/75K and 0Na/100K are shown in Fig. 12.

S_{LT} could not be calculated for the composition 50Na/50K because two phases ($Na_2CaSi_2O_6$ and K_2CaSiO_4) crystallize upon heating. Still, despite all the approximations that have been made, the S_{LT} values in Fig. 12 point to a MAE on sintering.

In another attempt to infer the densitication ability of the studied compositions, we also employed some glass stability (against crystallization) parameters, which only infer the crystallization kinetics and can be calculated from the characteristic temperatures obtained in a single DSC run. According to most of the GS parameters tested, Bioglass 45S5 has the lowest glass stability, i.e., lowest values of these GS parameters among the five tested compositions. This indicates that this composition should have the lowest sinterability. In fact, this is confirmed by its experimental sintering curve.

Analyzing the three best parameters (K_2, K_W, and K_H), the compositions 50Na/50K and 0Na/100K show the lowest tendency to crystallize. Hence, both compositions should exhibit similar sintering behaviors. However, the stability of the composition 0Na/100K against crystallization is not consistent with its low sinterability, since its densification reaches less than 3 %. After the heating and cooling cycle, as observed in the case of Bioglass 45S5, the particles still present sharp edges and few contact points; therefore, the measured "densification" can be attributed to partial crystallization of the particles.

There is no clear correlation between the GS parameters tested and the sintering results. They fail for the composition with the highest content of K_2O. The GS parameters tested fail in predicting the sintering ability because they consider only the crystallization tendency, while viscosity effects are neglected. Additionally, they are best suited for stoichiometric compositions or at least, for compositions that crystallize only in one crystal phase.

4.2. Effects on the viscosity

In the early 1940s, Poole et al. [60,61] were one of the first to investigate the effect of substitution of Na_2O by K_2O on the viscosity of glasses in the system Na_2O-K_2O-SiO_2. Poole identified an MAE on viscosity at low temperatures, especially near the laboratory T_g ($\eta = 10^{12}$ Pa.s), as shown in Fig. 13. As a result of the MAE, the working range of the glass is considerably increased. However, at high temperatures near the molten state, the minimum of the viscosity is less apparent, as was

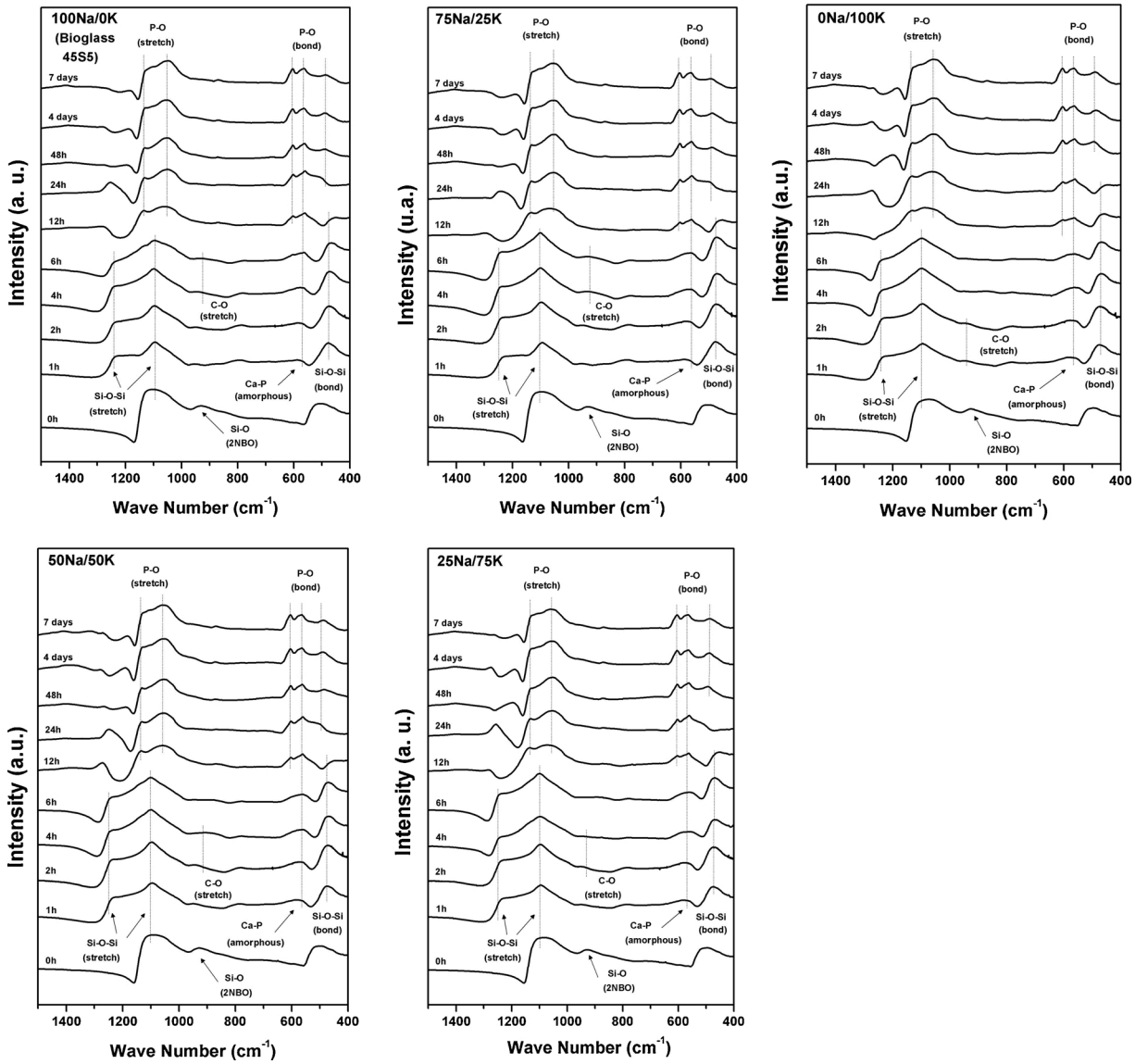

Fig. 9. FTIR spectra of the compositions 100Na/0K (Bioglass 45S5), 75Na/25K, 50Na/50K, 25Na/75K, and 0Na/100K, exposed to an SBF solution from 1 h to 7 days.

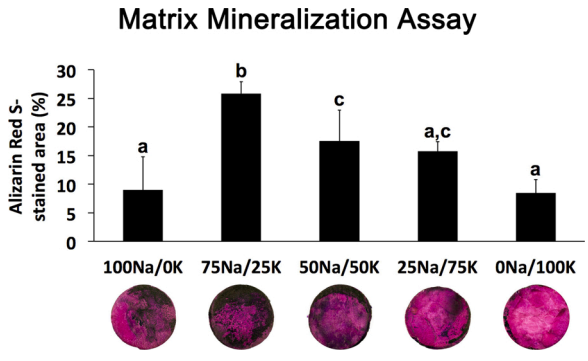

Fig. 10. Proportion of Alizarin Red S-stained area in MC3T3-E1 cell cultures grown for 21 days on the following surface compositions: 100Na/0K (Bioglass 45S5), 75Na/25K, 50Na/50K, 25Na/75K, and 0Na/100K. The macroscopic images of the ARS-stained cultures on the various glass disc compositions are presented below each bar. Bars that share 1 letter are not significantly ($P > 0.05$) different from each other (one-way ANOVA, Holm–Sidak test) (For interpretation of the references to colour in this figure legend, the reader is referred to the web version of this article).

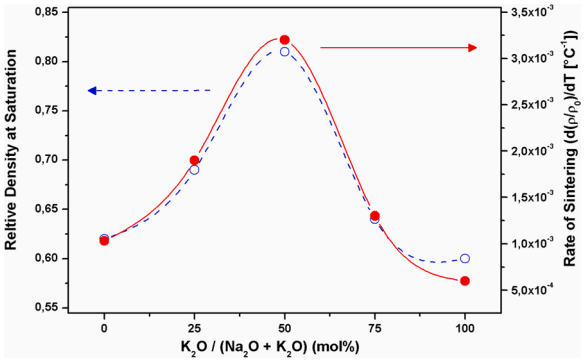

Fig. 11. Density at saturation, ρ_{sat} (dashed line) and rate of sintering, $d\frac{(p/p_0)}{dT}$(solid line) as a function of the percentage of Na_2O replaced by K_2O in Bioglass 45S5.

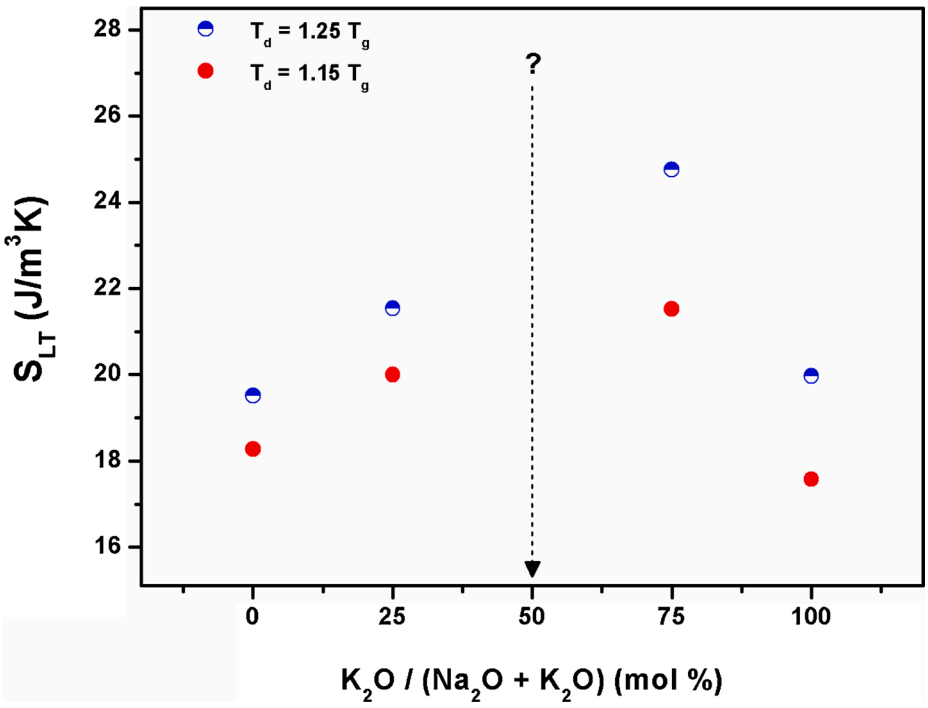

Fig. 12. Calculated values of S_{LT} for the Bioglass-based compositions, using Eq. 9 and two values of T_d ($T_d = 1.15T_g$ and $1.25T_g$).

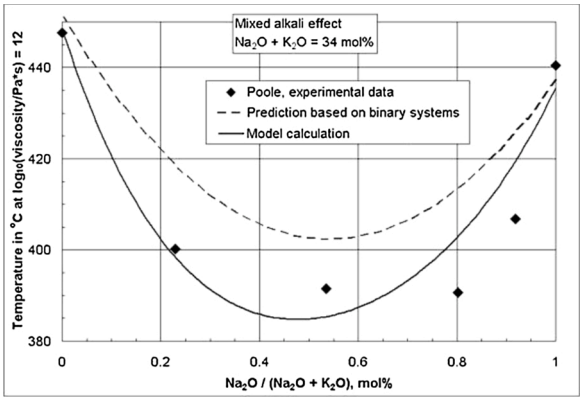

Fig. 13. MAE on the viscosity of glasses in the ternary glass Na_2O-K_2O-SiO_2, at log**η**(Pa.s) = 12. Figure extracted from Fluegel [63]. Experimental data extracted from Poole et al. [60,61].

experimentally observed by Gehlhoff and Thomas [62]. Later, Fluegel [63] developed a model for the calculation of viscosity as a function of composition for glasses in the same system. As shown in Fig. 13, calculations by Fluegel's model resulted in good agreement with the experimental data of Poole.

The experimental viscosity curves (Fig. 8) show that the substitution of Na_2O by K_2O promotes a gradual drop of viscosity in the temperature range where viscous flow sintering occurs (540–640 °C). The composition 50Na/50K exhibits the lowest values of viscosity at all temperatures. The viscosity of the glass 0Na/100K is significantly higher in the temperature range (600−660 °C, $T_{onset} - T_{sat}$) used for sintering, which justifies its poor densification. The higher viscosity of Bioglass also explains the absence of sintering before crystallization. In the sintering curves (Fig. 5), it is also possible to note that the compositions 75Na/25K and 50Na/50K start to densify at lower temperatures (T_{onset} = 530 °C, see Table 7) as a result of the lower viscosity. At the same temperature, the difference of viscosity between the compositions 0Na/100K and 50Na/50K reaches two orders of magnitude. Since Gehlhoff and Thomas [62] observed that the MAE is less evident at higher temperatures, it would be of great interest to know if this effect persists at lower viscosities.

Many theories have been proposed to explain the MAE, but none has received universal acceptance. Most of these theories were developed specifically to explain the effect on electrical conductivity (controlled by alkalis migration). However, viscosity does not depend simply on the cationic mobility, but also and much more on cooperative diffusion processes of the glass-forming cations (Si and O) or "structural units" or "cooperatively rearranging regions" (CRR), which can be much larger than the isolated cations. While electrical conductivity or alkali diffusivity exhibit minima, fluidity shows maxima in mixed alkali glasses [63,64]. This is not unreasonable since the structural units involved in alkali diffusion and viscous flow are different. A proof of this is the inability of the Stokes-Einstein relation to correlate viscosity and the alkali diffusivity [65,66]. Roughly, early models to explain the MAE considered structural differences between single and mixed alkali glasses, such as chemical heterogeneities or specific interactions between different cations, which lower their mobility. The latter effect could explain, for example, the reduction of crystal growth rates, since one cation would limit the movement of the other, diminishing the overall diffusion coefficient, as has been found for some binary silicate glasses [32]; however, the question of whether these models can be applied to explain the decrease of viscosity remains open to conjecture.

For instance, according to Fluegel [63], the MAE must be considered separately for viscosity and electrical conductivity. Based on a statistical modeling approach, Fluegel reasonably suggested that the MAE on the viscosity of silicates could be related to alkali-silica interactions rather than alkali-alkali interactions.

Using an approach based on the Adam-Gibbs theory, Richet [64] proposed a simple rationale to explain the MAE in silicate liquids. According to Richet, the mixing of alkalis in silicates increases the configurational entropy (S_c) of the system, which leads to a decrease in viscosity. In the Adam-Gibbs theory, viscosity can be described as a function of temperature, as follows:

$$\eta = A \exp\left(\frac{B}{T\, S_{c(T)}}\right) \tag{10}$$

where η is the viscosity, A and B are constants, T is the temperature, and S_{conf} is the configurational entropy of the liquid.

Taking logarithms of Eq. 10, one can derive:

$$Ln(\eta) = Ln(A) + \frac{B}{TS_{c(T)}} \quad (11)$$

Assuming that $\Delta Cp = \Delta Cp_{(liquid)} - \Delta Cp_{(glass)}$ represents the configurational heat capacity of the liquid, S_c can be described by

$$S_c(T) = S_c(T_f) + \int_{T_f}^{T} \frac{\Delta C_p}{T} dT \quad (12)$$

where T_f is the fictive temperature of the supercooled liquid (which for normal conditions is close to T_g).

It can be deduced from Eq. 11 that the deviation from Arrhenius behavior increases with the temperature dependence of S_c. To test the quantitative validity of this explanation, Richet used Eq. 11 and thermodynamic data available for $Na_2Si_3O_7$ (or Na_2O-$3SiO_2$) to calculate isothermal viscosities of liquid solutions in the $xNa_2Si_3O_7$-(1-x)$M_2Si_3O_7$ system (where $M_2Si_3O_7$ is a hypothetical amorphous alkali silicate which would have the same viscosity-temperature relationship as $Na_2Si_3O_7$). For intermediate compositions, a term for the configurational entropy of mixing ($\Delta_m S_c$) was added to Eq. 12. In the approximate case of a regular binary solution NS_n - MS_n, this term is given by

$$\Delta_m S_c = -R[X_{NSn} \ln(X_{NSn}) + (1 - X_{NSn}) \ln(1 - X_{NSn})] \quad (13)$$

where R is the gas constant, and X_{NSn} is the molar fraction of NS_n.

The calculated viscosities as a function of the composition are shown as dashed lines in Fig. 14. By fitting the Vogel-Fulcher-Tammann (VFT) equation to the experimental viscosity data, Richet also calculated the viscosity of some compositions in the Na_2O-K_2O-SiO_2 system (data points – Fig. 14). The solid lines represent a linear variation of composition with log viscosity, i.e., considering viscosity as an additive property. Fig. 14 shows that the calculated viscosities (dashed lines) mimic the deviations from additivity in the Na_2O-K_2O-SiO_2 system fairly well, representing an upper bound for the experimental viscosity values. Complete accuracy was not possible, according to Richet, because the viscosity of the composition $K_2Si_3O_7$ is higher than that of $Na_2Si_3O_7$. This effect is more pronounced at low temperatures near T_g. At higher temperatures, S_c decreases, and the deviation from additivity is less apparent. As mentioned before, this is in accordance with the experimental viscosity data obtained by Gehlhoff and Thomas [62]. Additionally, as correctly suspected by Day [32], the magnitude of the MAE is larger at low temperatures and for compositions with high alkali concentrations, which is the case for bioactive glasses.

Up to this point, it has been assumed that the viscosity of the parent glass controls the sintering process. However, the effective viscosity of the glass matrix likely changes due to crystallization; therefore, two complicating factors have been neglected: (1) viscosity changes as the glass partially crystallizes, since the composition of the residual glass phase is altered and (2) the presence of crystals in a glassy matrix additionally increases the overall (macroscopic) viscosity of the "composite". As mentioned previously, SEM micrographs of partially sintered glasses of the composition 25Na/75K (Fig. 6 – *g* and *h*) show many small crystals inside the particles. Müller et al. [67] showed that the effective viscosity of borosilicate glass increases with the increase of the volume fraction of alumina particles. Thus, the increase in effective viscosity due to internal crystallization may contribute to hindering viscous flow, especially in the composition 25Na/75K.

In addition to crystal growth rate and viscosity, another composition-dependent parameter that affects sintering is the glass-vapor surface energy (γ). Studies by Prado et al. [54–56] and all theoretical models of viscous flow sintering show that high values of γ favor sintering. Calculated values of γ (Table 6) indicate that the replacement of Na_2O by K_2O reduces γ from approximately 0.34 J/m^2 (composition 100Na/0K) to 0.24 J/m^2 (composition 0Na/100K). The reduction (~30 %) is significant, and thus, K_2O-rich compositions should exhibit a lower sinterability than Bioglass 45S5.

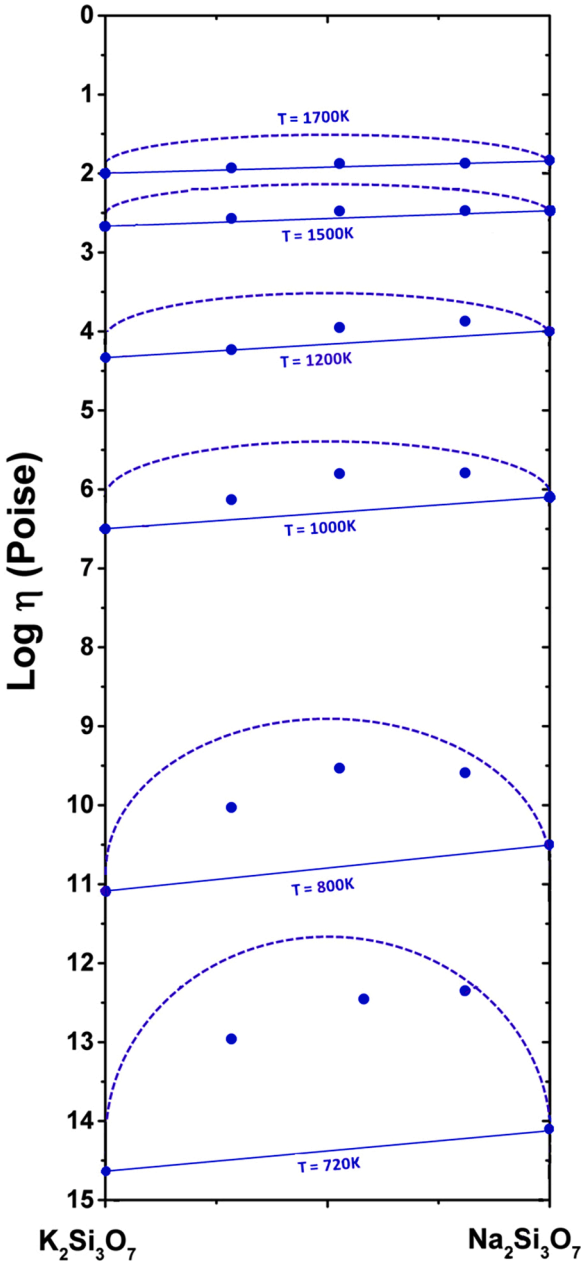

Fig. 14. Viscosity as a function of composition for alkali silicate melts. Data points (●) were estimated using the VFT equation, adjusted to experimental data. Solid lines: Viscosities of $xNa_2Si_3O_7$-(1-x)$K_2Si_3O_7$ predicted in the case of a linear variation of log viscosity with composition. Dashed lines: Calculated Isothermal viscosities of liquid solutions $xNa_2Si_3O_7$-(1-x)$M_2Si_3O_7$. Adapted from reference [64].

There are a few sintering models that describe the process of sintering with concurrent crystallization in non-isothermal conditions [68–71]. Among these, the *Clusters model* [56,72] has been proven to show a good agreement between calculated and experimental data. According to this model, if one considers only the Frenkel stage of sintering (the initial 10 % of densification), the evolution of a glass particle compact density in non-isothermal sintering can be described as

$$\rho_{c,F}(T) = \frac{\rho_0}{\left[1 - \frac{3\gamma K_s}{8 r q} \int_{T_g}^{T} \frac{1-\alpha_s(T')}{\eta(T')} dT'\right]^3} \quad (14)$$

where $\rho_{C,F}$ is the density of a powder compact at a given temperature (considering only the Frenkel stage of sintering), ρ_0 is the initial (green) density of the powder compact, γ is the glass-vapor surface energy, K_S is a particle shape factor (which account for the deviation from spherical shape), r is the average particle radius, q is the heating rate, T_g is the glass transition temperature, and η is the viscosity at a given temperature.

The parameter α_S, presented in Eq. 14, is the crystallized fraction at the surface of each glass particle at a given temperature and can be described by Eq. 15, derived from the JMAK theory [72]:

$$\alpha_s(T) = 1 - e^{-\pi\frac{N_S}{q^2}\left(\int_{T_g}^{T} U(T')dT'\right)^2} \quad (15)$$

where N_s is the number of preferential sites for surface nucleation, $U(T)$ is the crystal growth rate, and q is the heating rate (assumed to be constant). An analysis of Eq. 14 shows that the effects of U and η on sintering surpass any effect of γ, and thus are the main parameters controlling that phenomenon.

The results presented in this work show that the *mixed alkali effect* promotes a decisive decrease of crystallization, enhancing the glass stability against crystallization and diminishing the glass viscosity, which allows for densification driven by viscous flow.

4.3. In vitro behavior

Substitution of Na_2O by K_2O did not affect the *in vitro* bioactivity of the studied compositions, as assessed by immersion in SBF. Fig. 9 shows that the sequence of reactions is practically the same for all compositions. The reactions follow the main stages of formation of HCA, proposed by Hench [17,73], who observed the initial precipitation of a silica gel layer on the glass surface, followed by the deposition of an amorphous Ca-P layer and its subsequent crystallization into HCA. Peitl et al. [74] considered the appearance of the second peak of the P—O bond at 602 cm^{-1} as the onset of HCA formation. If one uses this criterion, for all studied compositions, the HCA phase starts to form on the glass surface after 12 h exposure to SBF. As mentioned in item 3.6, after 24 h exposure, only peaks related to HCA can be identified, which confirm their high bioactivity.

In general, it is accepted that mixed alkali glasses exhibit lower solubility than single-alkali glasses [32]. The reason is that in aqueous solutions, the solubility depends partially on the rate of exchange of alkali ions with H^+ ions from the solution. It has long been known that alkali ion mobility is lower in mixed alkali glasses. Therefore, the solubility is expected to be lower. However, one must consider that the *in vitro* test using the SBF solution gives only an indirect idea of solubility. It is well established that the mechanism of HCA formation on bioactive glasses depends not only on the exchange of alkali ions by H^+ but also on the breakage of Si-O-Si bonds and complex mechanisms of precipitation of silica gel and amorphous calcium phosphate, preceding the crystallization of HCA. If the composition 50Na/50K, in fact, shows a lower solubility, this difference is not sufficiently high to affect either the onset time for HCA formation or its further development.

Although no significant changes were detected in the HCA formation among the various glass compositions, the matrix mineralization of MC3T3-E1 cultures was enhanced on the 75Na/25K and 50Na/50K compared with the single-alkali glasses. These non-corresponding results were not unexpected, since the SBF test is not an accurate indicator of the bioactive potential of glasses when interacting with biological tissues [75–77]. One possible explanation for the enhancement in the osteogenic potential of pre-osteoblastic cells on two mixed alkali compositions lies in the patterns of dissolution behavior, which likely differ from those of the 100Na/0K and 0Na/100K glasses [78], favoring the achievement of mature osteoblastic phenotypes in MC3T3-E1 cultures and eventually the production of a mineralized matrix by these cells. The potential increase in extracellular K^+ in the cultures grown on 75Na/25K and 50Na/50K glasses could inhibit the efflux of intracellular K^+, which ultimately lead to inhibition of apoptosis and stimulation of osteoblastic cell proliferation (discussed in [79,80]). The formation of denser areas of matrix mineralization, i.e., the dark-brownish irregular areas that were observed in higher quantities on 75Na/25K and 50Na/50K glasses, supports that interpretation and was comparable to that described for other bioactive material surfaces [81].

Therefore, partial substitution of Na_2O by K_2O is an efficient strategy to improve the sinterability of compositions within the Na_2O-K_2O-CaO-SiO_2-P_2O_5 system, without the necessity of increasing the content of network formers, which typically would impair bioactivity.

5. Conclusions

In this work we demonstrated that the replacement of Na_2O by K_2O decreases both the crystallization kinetics and the viscosity of glass compositions in the $24.4(xNa_2O\text{-}(1\text{-}x)K_2O\text{-}26.9CaO\text{-}46.1SiO_2\text{-}2.6P_2O_5$ system (mol%, where x = 1, 0.75, 0.5, 0.25 and 0). The composition in which half the Na_2O was replaced by K_2O (50Na/50K) achieved the highest densification in the shortest time. This result confirms the mixed alkali effect (MAE) on the sintering kinetics. We also developed a new parameter (S_{LT}), which is valid for deep supercoolings, and correctly predicted the densification tendency of the studied glasses. The compositional change did not affect the HCA formation ability in SBF solution, but enhanced the osteogenic potential of pre-osteoblastic cells. These results are very relevant for this particular glass system, and also for the design of new bioactive glass compositions having improved sinterability and *in vitro* performance.

Declaration of Competing Interest

The authors declare that they have no known competing financial interests or personal relationships that could have appeared to influence the work reported in this paper.

Acknowledgments

The authors would like to thank the CNPq - Brazil, the São Paulo Research Foundation - FAPESP process nº 2008/11539-0, process nº 2013/07059-0 and CeRTEV (Center for Research, Technology, and Education in Vitreous Materials – process FAPESP n° 2013/07793-6) for generous and continuous funding. This study was also financed in part by the Coordenação de Aperfeiçoamento de Pessoal de Nível Superior (CAPES - Brazil) - Finance Code 001.

References

[1] L.L. Hench, The story of bioglass®, J. Mater. Sci. Mater. Med. 17 (11) (2006) 967–978.
[2] I.D. Xynos, et al., Gene-expression profiling of human osteoblasts following treatment with the ionic products of bioglass® 45S5 dissolution, J. Biomed. Mater. Res. 55a (2001) 151–157.
[3] L.L. Hench, J.M. Polak, Third-generation biomedical materials, Science 295 (2002) 1014–1017.
[4] J.R. Jones, Review of bioactive glass: from Hench to hybrids, Acta Biomater. 9 (1) (2013) 4457–4486.
[5] R.M. Day, Bioactive glass stimulates the secretion of angiogenic growth factors and angiogenesis in vitro, Tissue Eng. 11 (5-6) (2005) 768–777.
[6] A.A. Gorustovich, J.A. Roether, A.R. Boccaccini, Effect of bioactive glasses on angiogenesis: a review of in vitro and in vivo evidences, Tissue Eng. Part B Rev. 16 (2) (2010) 199–207.
[7] A. Arkudas, et al., Evaluation of angiogenesis of bioactive glass in the arteriovenous loop model, Tissue Eng. Part C Methods 19 (6) (2013) 479–486.
[8] M. Bellantone, N.J. Coleman, L.L. Hench, Bacteriostatic action of a novel four-component bioactive glass, Journal of Biomedical Materials Research - Part A 51 (3) (2000) 484–490.
[9] I. Allan, H. Newman, M. Wilson, Antibacterial activity of particulate bioglass® against supra- and subgingival bacteria, Biomaterials 22 (2001) 1683–1687.
[10] J.R. Jones, et al., Controlling ion release from bioactive glass foam scaffolds with antibacterial properties, J. Mater. Sci. Mater. Med. 17 (2006) 989–996.
[11] D. Zhang, et al., Factors controlling antibacterial properties of bioactive glasses, Key Eng. Mater. 330-332 (2007) 173–176.

[12] E. Munukka, et al., Bactericidal effects of bioactive glasses on clinically important aerobic bacteria, J. Mater. Sci. Mater. Med. 19 (1) (2008) 27–32.
[13] D.C. Clupper, L.L. Hench, Crystallization kinetics of tape cast bioactive glass 45S5, J. Non. Solids 318 (1-2) (2003) 43–48.
[14] A.R. Boccaccini, D.S. Brauer, L. Hupa (Eds.), Bioactive Glasses: Fundamentals, Technology and Applications, vol.23, Royal Society of Chemistry, 2016.
[15] M. Tylkowski, D.S. Brauer, Mixed alkali effects in bioglass® 45S5, J. Non. Solids 376 (2013) 175–181.
[16] I. Elgayar, et al., Structural analysis of bioactive glasses, J. Non. Solids 351 (2) (2005) 173–183.
[17] L.L. Hench, J. Wilson, An Introduction to Bioceramics (2nd Edition), World Scientific Publishing, Florida (USA), 1993.
[18] D. Bellucci, A. Sola, V. Cannillo, Low temperature sintering of innovative bioactive glasses, J. Am. Ceram. Soc. 95 (4) (2012) 1313–1319.
[19] M.R. Filgueiras, G. La Torre, L.L. Hench, Solution effects on the surface reactions of a bioactive glass, J. Biomed. Mater. Res. 27 (4) (1993) 445–453.
[20] M. Brink, et al., Compositional dependence of bioactivity of glasses in the system Na_2O-K_2O-CaO-MgO-SiO_2-P_2O_5-B_2O_3, Journal of Biomedical Materials Research – Part A 37 (1) (1997) 114–121.
[21] M. Brink; K. Karlsson; A. Yli-urpo. Bioactive glasses and their use. Patent number WO96/21628 (US6054400A), 1996.
[22] S.M. Salman, S.N. Salama, H.A. Abo-Mosallan, The role of strontium and potassium on crystallization and bioactivity of Na_2O-CaO-P_2O_5-SiO_2 glasses, Ceram. Int. 38 (2012) 55–63.
[23] K.L. Tucker, Potassium, magnesium and fruit and vegetables intakes are associated with greater bone mineral density in elderly men and women, Am. J. Clin. Nutr. 69 (1999) 727–736.
[24] K. Zhu, A. Devine, R.L. Prince, The effects of high potassium consumption on bone mineral density in a prospective cohort study of elderly postmenopausal women, Osteoporos. Int. 20 (2009) 335–340.
[25] M.J. Pascual, A. Durán, M.O. Prado, A new method for determining fixed viscosity points of glasses, Phys. Chem. Glasses – Eur. J. Glass Sci. Technol. Part B 46 (5) (2005) 512–520.
[26] E.D. Zanotto, Viscosidade de vidros pelo método de penetração – parte I, Cermica 29 (1983) 135–139.
[27] T. Kokubo, H. Kushitani, Solutions able to reproduce in vivo surface- structure changes in bioactive glass-ceramic A/W, J. Biomed. Mater. Res. 24 (6) (1990) 721–734.
[28] Y.L. Bruni, et al., Effects of surface treatments on Y-TZP phase stability, microstructure and osteoblast cell response, Ceram. Int. 41 (10) (2015) 14212–14222.
[29] M.A. de Oliva, et al., Treatment with a growth factor-protein mixture inhibits formation of mineralized nodules in osteogenic cell cultures grown on titanium, J. Histochem. Cytochem. 57 (3) (2009) 265–276.
[30] R.M. Hakim, D.R. Uhlmann, On the mixed alkali effect in glasses, Phys. Chem. Glasses 8 (5) (1967) 174–177.
[31] R. Terai, The mixed alkali effect in the Na_2O-Cs_2O-SiO_2 glasses, J. Non. Solids 6 (1971) 121–135.
[32] D.E, Day Mixed alkali glasses: their properties and uses, J. Non. Solids 21 (1976) 343–372.
[33] Z.P. Lu, C.T. Liu, A new glass-forming ability criterion for bulk metallic glasses, Acta Mater. 50 (2002) 3501–3512.
[34] M.L.F. Nascimento, et al., Can glass stability parameters infer glass forming ability? J. Non. Solids 351 (2005) 3296–3308.
[35] D. Turnbull, Under what conditions can a glass be formed? Contemp. Phys. 10 (5) (1969) 473–488.
[36] M.C. Weinberg, An assessment of glass stability criteria, Phys. Chem. Glasses 35 (3) (1994) 119–123.
[37] A. Hruby, Evaluation of glass-forming tendency by means of DTA, Czechoslovak Journal of Physics B 22 (11) (1972) 1187–1193.
[38] M. Saad, M. Poulain, Glass forming ability criterion, Mater. Sci. Forum 19-20 (1987) 11–18.
[39] N. Lotfibakhshaiesh, D.S. Brauer, R.G. Hill, Bioactive glass engineered coatings for ti6al4v alloys: influence of strontium substitution for calcium on sintering behavior, J. Non. Solids 356 (44-49) (2010) 2583–2590.
[40] Z.Y. Wu, et al., Melt-derived bioactive glass scaffolds produced by a gel-cast foaming technique, Acta Biomater. 7 (4) (2011) 1807–1816.
[41] R. Comesaña, et al., Three-dimensional bioactive glass implants fabricated by rapid prototyping based on CO_2 laser cladding, Acta Biomater. 7 (9) (2011) 3476–3487.
[42] J.O. Isard, The mixed alkali effect in glass, J. Non-Crystalline Solids 1 (1969) 235–261.
[43] M.J. Jackson, Thermal expansion of alumino-alkali silicate and alumino-borosilicate glasses – comparison of empirical models, J. Mater. Sci. Lett. 16 (1997) 1264–1266.
[44] S. Knickerbocker, M.R. Tuzzolo, S. Lawhorne, Sinterable β-spodumene glass-ceramics, J. Am. Ceram. Soc. 72 (10) (1989) 1873–1879.
[45] D.C. Clupper, et al., Sintering temperature effects on the in vitro bioactive response of tape cast and sintered bioactive glass-ceramic in tris buffer, J. Biomed. Mater. Res. 57 (4) (2001) 532–540.
[46] D.C. Clupper, L.L. Hench, Crystallization kinetics of tape cast bioactive glass 45S5, J. Non. Solids 318 (1) (2003) 43–48.
[47] D.C. Clupper, L.L. Hench, J.J. Mecholsky, Strength and toughness of tape cast bioactive glass 45S5 following heat treatment, J. Eur. Ceram. Soc. 24 (10) (2004) 2929–2934.
[48] Q.Z. Chen, I.D. Thompson, A.R. Boccaccini, 45S5 bioglass®-derived glass-ceramic scaffolds for bone tissue engineering, Biomaterials 27 (2006) 2414–2425.
[49] Q.Z. Chen, A.R. Boccaccini, Poly (d, l-lactic acid) coated 45S5 bioglass®-based scaffolds: processing and characterization, J. Biomed. Mater. Res. Part A 77 (3) (2006) 445–457.
[50] Q.Z. Chen, et al., Surface functionalization of bioglass®-derived porous scaffolds, Acta Biomater. 3 (4) (2007) 551–562.
[51] A.L. Metze, et al., Gelatin coated 45S5 bioglass®-derived scaffolds for bone tissue engineering, Key Eng. Mater. 541 (2013) 31–39.
[52] L. Lefebvre, et al., Structural transformations of bioactive glass 45S5 with thermal treatments, Acta Mater. 55 (10) (2007) 3305–3313.
[53] R.G. Hill, D.S. Brauer, Predicting the bioactivity of glasses using the network connectivity or split network models, J. Non. Solids 357 (24) (2011) 3884–3887.
[54] E.D. Zanotto, M.O. Prado, Isothermal sintering with concurrent crystallisation of monodispersed and polydispersed glass particles. Part 1, Phys. Chem. Glasses – Eur. J. Glass Sci. Technol. Part B 42 (3) (2001) 191–198.
[55] M.O. Prado, C. Fredericci, E.D. Zanotto, Glass sintering with concurrent crystallisation. Part 2. Nonisothermal sintering of jagged polydispersed particles, Phys. Chem. Glasses – Eur. J. Glass Sci. Technol. Part B 43 (5) (2002) 215–223.
[56] M.O. Prado, C. Fredericci, E.D. Zanotto, Non-isothermal sintering with concurrent crystallization of polydispersed soda–lime–silica glass beads, J. Non. Solids 331 (1) (2003) 157–167.
[57] R. Müller, E.D. Zanotto, V.M. Fokin, Surface crystallization of silicate glasses: nucleation sites and kinetics, J. Non. Solids 274 (2000) 208–231.
[58] M.O. Prado, M.L.F. Nascimento, E.D. Zanotto, On the sinterability of crystallizing glass powders, J. Non. Solids 354 (2008) 4589–4597.
[59] J.W.P. Schmelzer, et al., Crystallization in glass-forming liquids: effects of decoupling of diffusion and viscosity on crystal growth, J. Non. Solids 429 (2015) 45–53.
[60] J.P. Poole, M. Gensamer, Systematic study of effect of oxide constituents on viscosity of silicate glasses at annealing temperatures, J. Am. Ceram. Soc. 32 (7) (1949) 220–229.
[61] J.P. Poole, Low-temperature viscosity of alkali silicate glasses, J. Am. Ceram. Soc. 32 (7) (1949) 230–233.
[62] G. Gehlhoff, M. Thomas, Physical properties of glass related to their composition: ii, mechanical properties, Zeitschrift für Technische Physik 7 (1926) 105–126.
[63] A. Fluegel, Glass viscosity calculation based on a global statistical modeling approach, Glass Technol. Eur. J. Glass Sci. Technol. A 48 (1) (2007) 13–30.
[64] P. Richet, Viscosity and configurational entropy of silicate melts, Geochim. Cosmochim. Acta 48 (1983) 471–483.
[65] A.W. Hofmann, Diffusion in natural silicate melts: a critical review, Phys. Magmatic Processes (1980) 385–417.
[66] M.L.F. Nascimento, et al., Dynamic processes in a silicate liquid from above melting to below the glass transition, J. Chem. Phys. 135 (19) (2011) 194703.
[67] R. Müller, et al., Effect of rigid inclusions on sintering of low temperature co-fired ceramics, Phys. Chem. Glasses – Eur. J. Glass Sci. Technol. Part B 48 (4) (2007) 259–266.
[68] T.J. Clark, J.S. Reed, Kinetic processes involved in the sintering and crystallization of glass powders, J. Am. Ceram. Soc. 69 (11) (1986) 837–846.
[69] S. Jagota, R. Raj, Model for the crystallization and sintering of unseeded and seeded boehmite gels, J. Mater. Sci. 27 (8) (1992) 2251–2257.
[70] M.O. Prado, E.D. Zanotto, Glass sintering with concurrent crystallization, Comptes Rendus Chim. 5 (11) (2002) 773–786.
[71] R. Huang, et al., A two-scale model for simultaneous sintering and crystallization of glass–ceramic scaffolds for tissue engineering, Acta Biomater. 4 (4) (2008) 1095–1103.
[72] V.O. Soares, et al., Non-isothermal sinter-crystallization of jagged Li_2O–Al_2O_3–SiO_2 glass and simulation using a modified form of the clusters model, J. Non. Solids 358 (23) (2012) 234–3242.
[73] L.L. Hench, Bioceramics: from concept to clinics, J. Am. Ceram. Soc. 74 (7) (1991) 1487–1510.
[74] O. Peitl, E.D. Zanotto, L.L. Hench, Highly bioactive P_2O_5-Na_2O-CaO-SiO_2 glass-ceramics, J. Non. Solids 292 (2001) 115–126.
[75] Q. Fu, M.N. Rahaman, D.E. Day, Accelerated conversion of silicate bioactive glass (13-93) to hydroxyapatite in aqueous phosphate solution containing polyanions, J. Am. Ceram. Soc. 92 (2009) 2870–2876.
[76] M. Bohner, J. Lemaitre, Can bioactivity be tested in vitro with SBF solution? Biomaterials 30 (12) (2009) 2175–2179.
[77] T. Kokubo, H. Takadama, How useful is SBF in predicting in vivo bone bioactivity? Biomaterials 27 (15) (2006) 2907–2915.
[78] C.W. Stokes, R. van Noort, R.J. Hand, Investigation of the chemical solubility of mixed-alkali fluorcanasite forming glasses, J. Non. Solids 352 (2) (2006) 142–149.
[79] L. Wang, et al., Proliferation and osteo/odontoblastic differentiation of stem cells from dental apical papilla in mineralization-inducing medium containing additional KH_2PO_4, Cell Prolif. 46 (2) (2013) 214–222.
[80] H. Kito, et al., Downregulation of the Ca^{2+}-activated K^+ channel $K_{Ca}3.1$ in mouse preosteoblast cells treated with vitamin D receptor agonist, Am. J. Physiol. Cell Physiol. 319 (2) (2020) C345–C358.
[81] K.K. Pereira, et al., Progression of osteogenic cell cultures grown on microtopographic titanium coated with calcium phosphate and functionalized with a type I collagen-derived peptide, J. Periodontol. 84 (8) (2013) 1199–1210.